06-09 June 2009

TECH BRIEFS

NATIONAL AERONAUTICS AND SPACE ADMINISTRATION

INTRODUCTION

Tech Briefs are short announcements of innovations originating from research and development activities of the National Aeronautics and Space Administration. They emphasize information considered likely to be transferable across industrial, regional, or disciplinary lines and are issued to encourage commercial application.

Availability of NASA Tech Briefs and TSPs

Requests for individual Tech Briefs or for Technical Support Packages (TSPs) announced herein should be addressed to

National Technology Transfer Center

Telephone No. **(800) 678-6882** or via World Wide Web at **www2.nttc.edu/leads/**

Please reference the control numbers appearing at the end of each Tech Brief. Information on NASA's Innovative Partnerships Program (IPP), its documents, and services is also available at the same facility or on the World Wide Web at **http://ipp.nasa.gov**.

Innovative Partnerships Offices are located at NASA field centers to provide technology-transfer access to industrial users. Inquiries can be made by contacting NASA field centers listed below.

Ames Research Center
Lisa L. Lockyer
(650) 604-1754
lisa.l.lockyer@nasa.gov

Dryden Flight Research Center
Gregory Poteat
(661) 276-3872
greg.poteat@dfrc.nasa.gov

Glenn Research Center
Kathy Needham
(216) 433-2802
kathleen.k.needham@nasa.gov

Goddard Space Flight Center
Nona Cheeks
(301) 286-5810
nona.k.cheeks@nasa.gov

Jet Propulsion Laboratory
Andrew Gray
(818) 354-3821
gray@jpl.nasa.gov

Johnson Space Center
information
(281) 483-3809
jsc.pechtran@mail.nasa.gov

Kennedy Space Center
David R. Makufka
(321) 867-6227
david.r.makufka@nasa.gov

Langley Research Center
Brian Beaton
(757) 864-2192
brian.f.beaton@nasa.gov

Marshall Space Flight Center
Jim Dowdy
(256) 544-7604
jim.dowdy@msfc.nasa.gov

Stennis Space Center
Ramona Travis
(228) 688-3832
ramona.e.travis@nasa.gov

Carl Ray, Program Executive
Small Business Innovation Research (SBIR) & Small Business Technology Transfer (STTR) Programs
(202) 358-4652
carl.g.ray@nasa.gov

Doug Comstock, Director
Innovative Partnerships Program Office
(202) 358-2560
doug.comstock@nasa.gov

06-09 June 2009

TECH BRIEFS

NATIONAL AERONAUTICS AND SPACE ADMINISTRATION

Device for Measuring Low Flow Speed in a Duct

Speed can be determined to within ±0.2 cm/s.

John H. Glenn Research Center, Cleveland, Ohio

A multiple-throat venturi system has been invented for measuring laminar flow of air or other gas at low speed (1 to 30 cm/s) in a duct while preserving the laminar nature of the flow and keeping the velocity profile across the duct as nearly flat as possible. While means for measuring flows at higher speeds are well established, heretofore, there have been no reliable means for making consistent, accurate measurements in this speed range. In the original application for which this system was invented, the duct leads into the test section of a low-speed wind tunnel wherein uniform, low-speed, laminar flow is required for scientific experiments. The system could also be used to monitor a slow flow of gas in an industrial process like chemical vapor deposition.

In the original application, the multiple-throat venturi system is mounted at the inlet end of the duct having a rectangular cross section of 19 by 14 cm, just upstream of an assembly of inlet screens and flow straighteners that help to suppress undesired flow fluctuations (see Figure 1). The basic venturi measurement principle is well established: One measures the difference in pressure between (1) a point just outside the inlet, where the pressure is highest and the kinetic energy lowest; and (2) the narrowest part (the throat) of the venturi passage, where the kinetic energy is highest and the pressure is lowest. Then by use of Bernoulli's equation for the relationship between pressure and kinetic energy, the volumetric flow speed in the duct can be calculated from the pressure difference and the inlet and throat widths.

The design of this system represents a compromise among length, pressure recovery, uniformity of flow, and complexity of assembly. Traditionally, venturis are used to measure faster flows in narrower cross sections, with longer upstream and downstream passages to maintain accuracy. The dimensions of the passages of the present venturi system are sized to provide a readily measurable pressure drop. Multiple throats are used to minimize the length needed to recover internal energy and enable the velocity profile to recover to near flatness. The venturi passages are defined by airfoil surfaces,

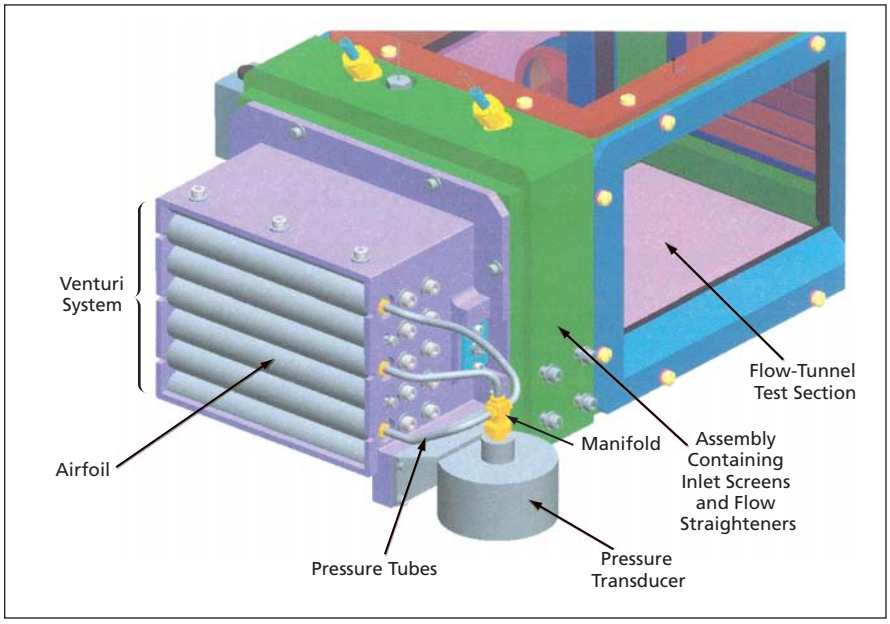

Figure 1. The **Multiple-Throat Venturi System** is mounted at the inlet end of a rectangular duct.

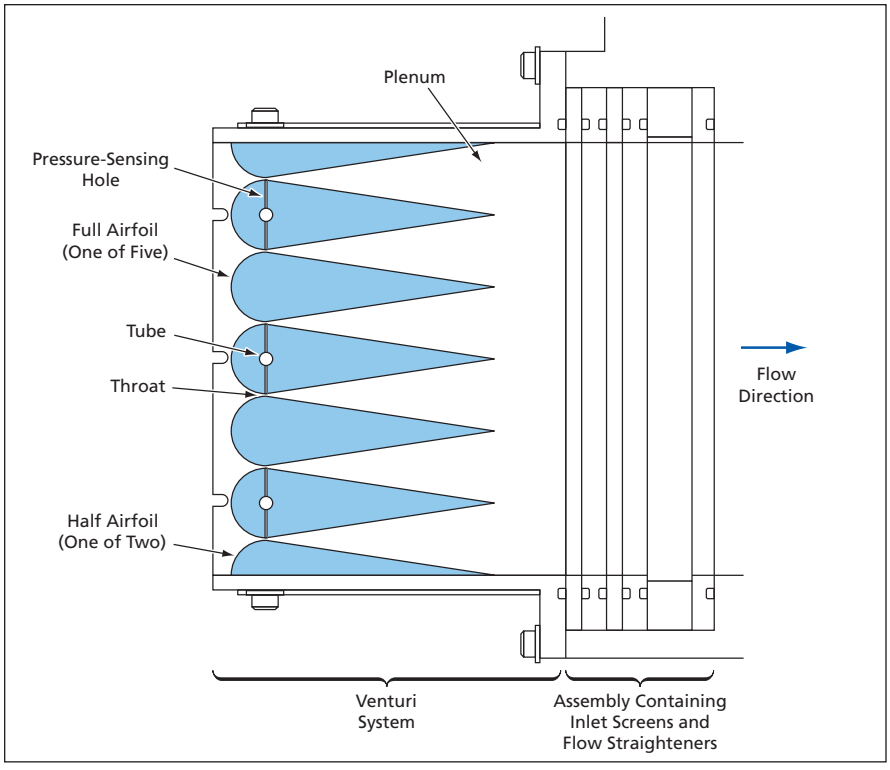

Figure 2. **Narrow Holes in Three of the Airfoils** connect pressure taps at the venturi throats with tubes, which, turn, connect the pressure taps to an input manifold of a differential-pressure sensor.

two-dimensional configuration of which is dictated by the need to match the rectangular duct cross section.

The flow into and out of the venturi passages is guided by the airfoil surfaces. There are two half airfoils at the top and bottom of the inlet, and there are five full airfoils between them. A plenum downstream of the trailing edges allows the flow to even out prior to entering the screens and flow straighteners. To enable measurement of pressure in all six throats, tubes in three of the airfoils are connected to a manifold, and narrow holes connecting the tubes with the throats are drilled in these airfoils. The pressures sensed at the six throat measurement locations become averaged together in the manifold, which is connected to one side of a sensitive differential-pressure transducer. The other side of the transducer is exposed to the pressure just upstream of the inlet. It has been found that the speed-vs.-pressure calibration curve is highly repeatable, enabling measurement of flow speed to within an error of ±0.2 cm/s.

This work was done by Frank Quinn and Kevin Magee of ZIN Technologies, Inc. for Glenn Research Center. Further information is contained in a TSP (see page 1).

Inquiries concerning rights for the commercial use of this invention should be addressed to NASA Glenn Research Center, Innovative Partnerships Office, Attn: Steve Fedor, Mail Stop 4–8, 21000 Brookpark Road, Cleveland, Ohio 44135. Refer to LEW-18021-1.

Measuring Thermal Conductivity of a Small Insulation Sample

Heat leakage is accounted for in design, operation, and calculation.

John H. Glenn Research Center, Cleveland, Ohio

An instrumentation system for direct measurement of the thermal conductivity of a small sample of a highly insulating material has been devised. As used here, (1) "small" signifies having dimensions of the order of two centimeters — significantly less than the sizes of specimens for which prior devices for direct measurement of thermal conductivity have been designed; and (2) "highly insulating" signifies having thermal conductivity of the order of that of air.

The heart of the system is an assembly that includes two copper disks — one electrically heated, the other cooled with chilled water. The disks are separated by a guard ring made of strong, thermally insulating polymethacrylamide foam. The sample fits between the copper disks and within the ring (see figure). Matched thermocouples are used to measure the temperatures of the heated and cooled disks. The heated and cooled disks are affixed to larger foam disks, and the essentially still air in the gap between the larger disks insulates the sides of the specimen. This air gap region can be further divided by extending the foam ring into the gap region. The entire assembly as described thus far is lightly clamped together by means of nylon threaded rods and is placed inside a cylindrical chamber wherein the temperature is maintained at a set value (typically, 25 °C).

The electric power supplied to the heated disk is adjusted to maintain the temperature of this disk at a fixed value (for example, 35 °C) that exceeds the temperature in the chamber by a fixed amount. Similarly, the supply of chilled water to the cooled disk is regulated to maintain the temperature in this disk at a

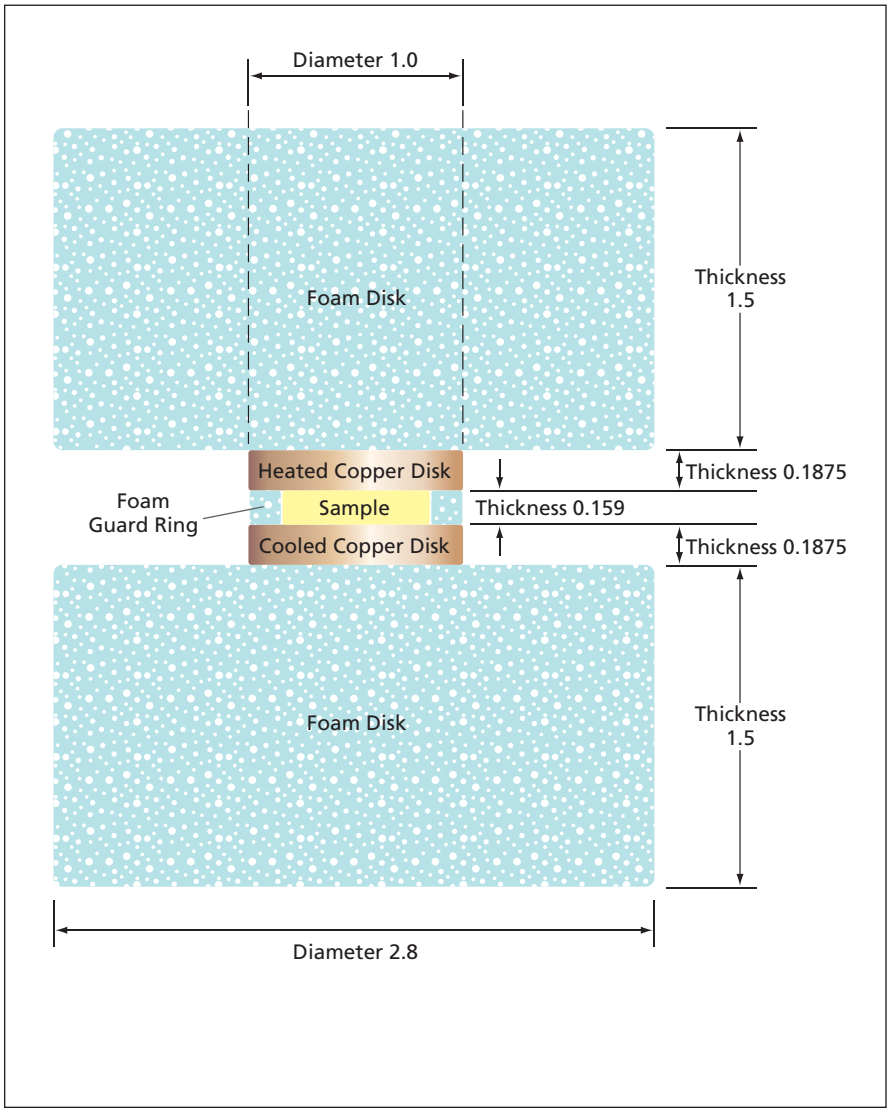

This Assembly is Mounted in a constant-temperature chamber. The heated and cooled disks are maintained at temperatures $\Delta T/2$ above and $\Delta T/2$ below, respectively, the chamber temperature. The thermal conductivity of the sample is determined from the heater power needed to maintain the $\Delta T/2$ temperature differential of the heated disk. (Note: The dimensions are in inches.)

value (in the present example, 15 °C) below the chamber temperature by the same fixed amount. Modeling shows that the resulting symmetry in the temperature differential, in combination with the geometric symmetry of the apparatus, serves to ensure that heat escaping from the edge of the heated disk flows through the air-gap region and, for the most part, returns to the edge of the cooled disk. It also ensures that the heat escaping from the half of the guard ring that is positioned toward the heated disk flows to the half of the guard ring positioned towards the cooled disk. This helps to assure one-dimensional heat flow through the sample, thereby minimizing the measurement errors. The time-averaged heater power needed to maintain the specified constant temperature of the heated disk in the steady state is what is measured.

The following description of the theory of operation and the calculation of thermal conductivity from measurement data is somewhat simplified for the sake of brevity. The heater power is nominally given by

$$Q = kA\Delta T/l + Q_L,$$

where k is the thermal conductivity of the sample material under test, A is the cross-sectional area of the sample (nominally, the area of the circle enclosed by the guard ring), ΔT is the specified difference between the temperatures of the heated and cooled disks, l is the thickness of the sample, and Q_L is the rate of leakage of heat along all paths other than that of direct one-dimensional thermal conduction through the thickness of the sample.

Modeling shows that the combination of temperature-differential and geometric symmetry and the one-dimensional heat flow through the sample ensures that the heat-leakage power is essentially independent of the sample material. Hence, it is possible to determine the value of Q_L as a function of the heated disk, cooled disk, and chamber wall temperatures from calibration measurements on one or more specimens having known thermal conductivities. Modeling also shows that the device may be calibrated using air as the reference standard material. Thereafter, one can use the value of Q_L as thus determined to calculate values of k from measured values of Q.

This work was done by Robert A Miller and Maria A Kuczmarski of Glenn Research Center. Further information is contained in a TSP (see page 1).

Inquiries concerning rights for the commercial use of this invention should be addressed to NASA Glenn Research Center, Innovative Partnerships Office, Attn: Steve Fedor, Mail Stop 4–8, 21000 Brookpark Road, Cleveland, Ohio 44135. Refer to LEW-18356-1.

Alignment Jig for the Precise Measurement of THz Radiation

This device can be used by optometrists to measure aberrations in lenses, and by head-mount display manufacturers.

NASA's Jet Propulsion Laboratory, Pasadena, California

An alignment jig (see figure) places a THz horn and power detector at the proper locations with respect to the focal points of a conic reflector in order to couple total power of the THz source radiating out of its horn into the power detector for precise measurement of its power. A visible laser beam locates focal points of the conic reflector. Measuring total diverging power from a THz point source is not an easy task. THz radiation has a wavelength range of between 0.1 and 1 mm. The power levels range from a few tens of nW to 100 mW. These power levels are low, and low temperatures (in the range of –173 °C) are typically used to house the THz power source. Because of the small target, the power emitter and the power detectors must be located in exact positions in order to fully capture the radiated energy. At these low powers, there are three common commercial power meters: a bolometer detector, a Golay Cell, and a Keating Meter. These three power meters have specific power ranges where they excel, and they must be calibrated at their overlapped power ranges. Because of the low THz power being measured, conical reflectors are used to send all of the radiated power to the detectors.

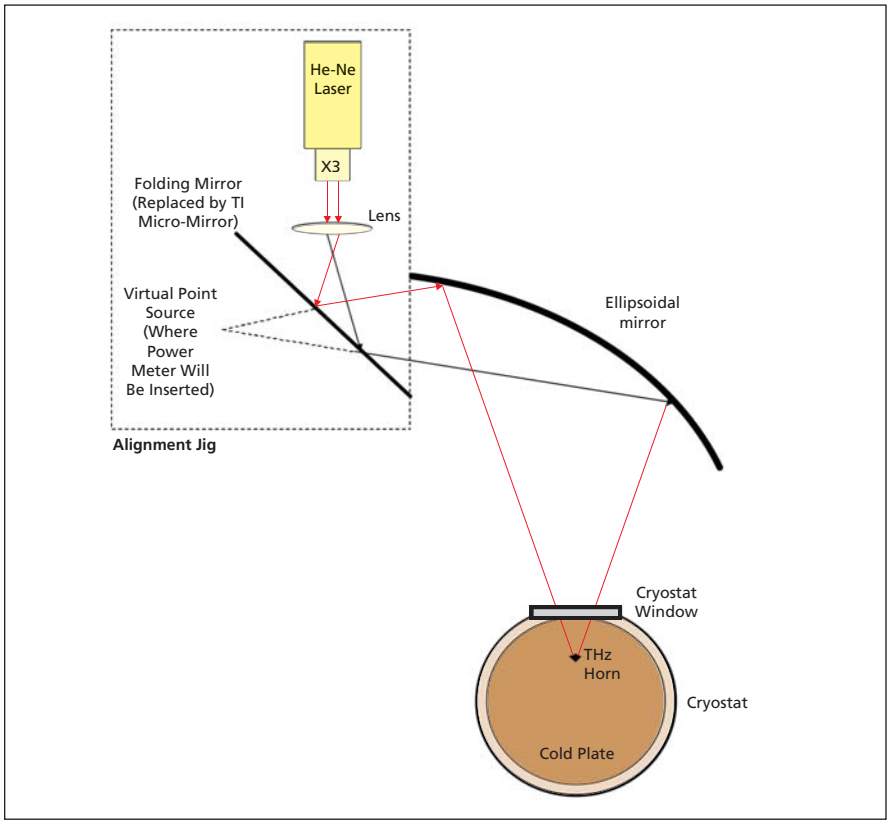

Figure 1. The **Alignment Jig** for measurement of THz power employs an ellipsoidal mirror with a THz horn at one focal point and the power meter at the second focal point.

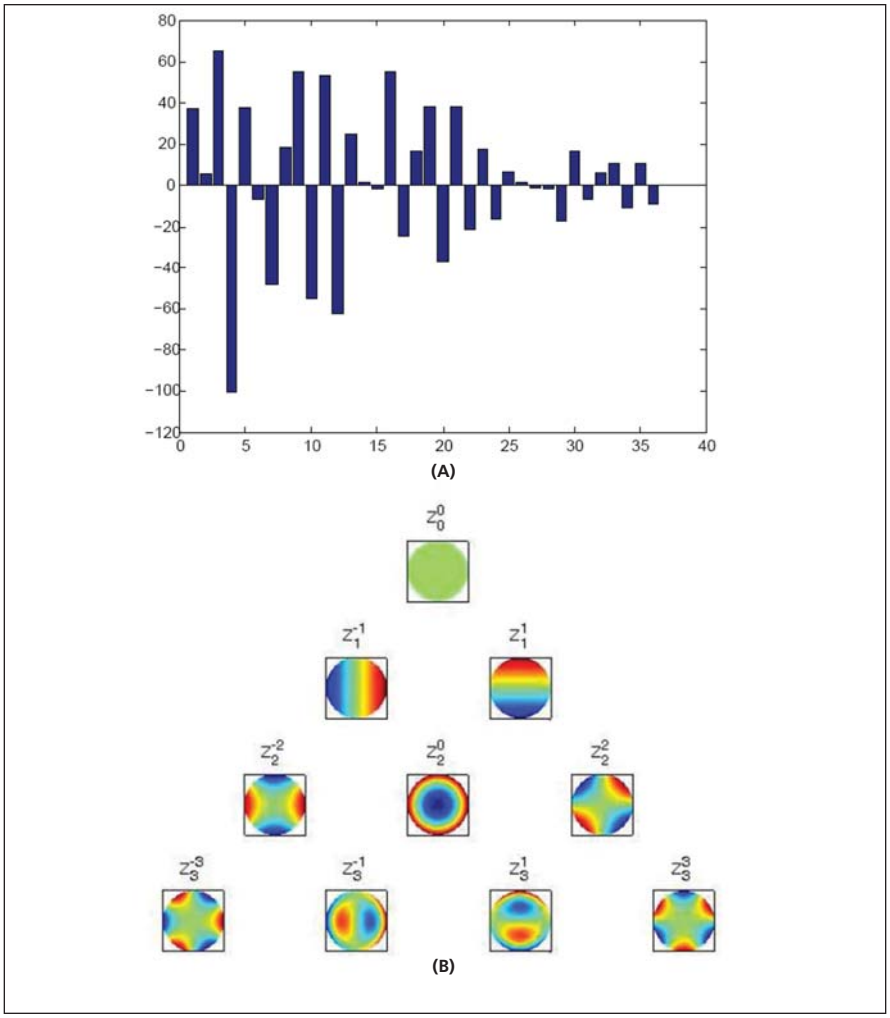

Figure 2. (a) **Quantification of Optical Aberration** as intorduced by an arbitrary lens is manifested by amplitude of its Zernicke coefficients specified in the order of (*n*= 0, 1, 2, 3, etc.: *m*=–*n*, . . . ,0, . . . , *n* if *n* even ; –*n*, . . . , *n* if *n* odd). (b) First 10 individual Zernicke functions are plotted.

These reflectors focus the energy of the THz source, and the detectors are placed at a convergent focal point to capture the radiated THz power.

One cannot place the detectors just by approximating by eye. THz waves are submillimeter, and require precise placement. The method proposed here is to use a visible low-power red laser (630 nm) with a 1-mm beam diameter (see Figure 1). The laser is beamed through a 3× beam expander to obtain a circular beam, then through a lens in order to focus the beam onto a TI DLP micro-mirror at an angle. This mirror bounces the laser light onto an ellipsoidal mirror that will focus it into a point. That is the point where the THz source is to be placed.

The initial focal point (laser source) is marked in 3D space as if the TI micro-mirror wasn't there. This virtual focal point is where the detector is to be placed. Since a circular beam is used, it is easier to locate the focal points by watching for the bright red spot that signals beam convergence.

Once the two focal points are found, and the energy source and energy detectors are in place, it is necessary to check calibration. Array of circular patterns can be beamed from the DLP chip to evaluate Zernike's refraction aberrations in real time (see Figure 2). In addition, various diagnostic patterns can be beamed from the DLP chip in order to measure aberrations associated with field variation. For example, a spot diagram can be beamed off of the DLP in order to analyze point spread.

This method is useful for the semiconductor industry to evaluate surface metrology of thin transparent optics, clinical optometry to measure lens aberration, telescopes and astronomical receivers to align mirrors covering optics and radiation sources, and head-mount displays to evaluate beam splitters.

This work was done by Hamid H. Javadi of Caltech for NASA's Jet Propulsion Laboratory. Further information is contained in a TSP (see page 1).

Autoignition Chamber for Remote Testing of Pyrotechnic Devices

This rugged, reusable chamber is portable and can remotely heat pyrotechnics for autoignition tests.

Lyndon B. Johnson Space Center, Houston, Texas

The autoignition chamber (AIC) performs by remotely heating pyrotechnic devices that can fit the inner diameter of the tube furnace. Two methods, a cold start or a hot start, can be used with this device in autoignition testing of pyrotechnics. A cold start means extending a pyrotechnic device into the cold autoignition chamber and then heating the device until autoignition occurs. A hot start means heating the autoignition chamber to a specified temperature, and then extending the device into a hot autoignition chamber until autoignition occurs. Personnel are remote from the chamber during the extension into the hot chamber.

The autoignition chamber, a commercially produced tubular furnace, has a 230-V, single-phase, 60-Hz electrical supply, with a total power output of 2,400 W. It has a 6-in. (15.2-cm) inner diameter, a 12-in. (30.4-cm) outer diameter and a 12-in.-long (30.4-cm), single-zone, solid tubular furnace (element) capable of heating to temperatures up to 2,012 °F (1,100 °C) in air. The furnace temperature is controlled by a commercial single-zone, setpoint temperature controller and solid-state relay.

The furnace features a stainless steel shell with 1/4-in.-thick (6-mm) steel end plates, and a rugged insulation package. A thermocouple port is supplied in the center of the control zone.

The furnace has a 2.5-in.-long (6.4-cm) vestibule at the top and bottom. The approximate overall length of the furnace is 17.5 in. (44.5 cm). Thermocouples on the pyrotechnic device monitor its temperature during the heating process on a strip chart recorder, or an equivalent data acquisition system. A remotely actuated ceramic protective cover is installed on top of the auto ignition chamber when test personnel are working around it.

A cage is mounted to a 115-VAC 500-lb (2,224-N) force electromechanical actuator that has an 18-in. (46-cm) stroke. The pyrotechnic device is installed in an appropriate mounting fixture, which is then installed in the cage. The actuator can be remotely operated to extend or retract the pyrotechnic device into the tube furnace. When the actuator is completely extended into the autoignition chamber, a ceramic insulating lid sits on top of the chamber to keep heat from escaping.

An accelerometer is installed on the stainless steal fixture of the electromechanical actuator to record the autoignition event. A strip chart recorder, or equivalent data acquisition system, monitors the accelerometer output. The chamber is capable of withstanding stress while still being able to function. In one instance of STS-107 Pyrotechnic Hardware, the autoignition chamber was reused a total of 18 times and did not require rebuilding.

This work was done by Maureen L. Harrington and Gerald R. Steward of Johnson Space Center, and Toby W. Dartez of Jacobs Sverdrup Corp. For further information, contact the JSC Innovation Partnerships Office at (281) 483-3809. MSC-24433-1

Microwave Power Combiners for Signals of Arbitrary Amplitude

Output polarization would no longer vary with input amplitudes.

NASA's Jet Propulsion Laboratory, Pasadena, California

Schemes for combining power from coherent microwave sources of arbitrary (unequal or equal) amplitude have been proposed. Most prior microwave-power-combining schemes are limited to sources of equal amplitude.

The basic principle of the schemes now proposed is to use quasi-optical components to manipulate the polarizations and phases of two arbitrary-amplitude input signals in such a way as to combine them into one output signal having a specified, fixed polarization. To combine power from more than two sources, one could use multiple power-combining stages based on this principle, feeding the outputs of lower-power stages as inputs to higher-power stages.

Quasi-optical components suitable for implementing these schemes include grids of parallel wires, vane polarizers, and a variety of waveguide structures. For the sake of brevity, the remainder of this article illustrates the basic principle by focusing on one scheme in which a wire grid and two vane polarizers would be used.

Wire grids are the key quasi-optical elements in many prior equal-power combiners. In somewhat oversimplified terms, a wire grid reflects an incident beam having an electric field parallel to the wires and passes an incident beam having an electric field perpendicular to the wires. In a typical prior equal-power combining scheme, one provides for two properly phased, equal-amplitude signals having mutually perpendicular linear polarizations to impinge from two mutually perpendicular directions on a wire grid in a plane oriented at an angle of 45° with respect to both beam axes. The wires in the grid are oriented to pass one of the incident beams straight through onto the output path and to reflect the other incident beam onto the output path along with the first-mentioned beam.

In the ideal case, the output beam contains the sum of the input beam powers and has linear polarization at an angle of 45° with respect to either of the input polarizations. Although ordinarily used to combine input signals of equal amplitude, this scheme still works when the amplitudes are unequal, except that undesirably, the output polarization is not fixed at 45°: instead, the angle of the output polarization, relative to the polarization of input signal 1, is given by $\arctan(E_1/E_2)$, where E_1 and E_2 are the electric-field amplitudes of the first and second input signals, respectively. According to the scheme now proposed, one would use a wire-grid combiner as in the equal-power case described above, in combination with two vane polarizers (see figure) that, as described below, would ensure that the output beam had the desired 45° linear polarization.

A vane polarizer (also known as a venetian-blind polarizer) consists of a number of thin metal strips that are parallel to each other. When the electric field of an incident beam is perpendicular to the strips, the field does not induce any electric current in the strips and so the beam passes through the strips, unaffected, in the transverse electromagnetic (TEM) mode. When the electric field is parallel to the strips, the beam is forced into the first transverse electric (TE_1) mode, which has a wavelength longer than that of the TEM mode. The thickness of the vane polarizer is chosen so that the TEM mode is delayed by a phase difference of 90° more than that of the TE_1 mode. When the incident beam is polarized at 45° to the vanes, the beam is split into two equal components, one of which is delayed by 90° relative to the other. Upon recombination of the components at the output, the resultant beam is circularly polarized. Conversely, when the incident beam is circularly polarized, the output beam is linearly polarized at 45°.

In the proposed scheme, the two vane polarizers would be placed in the output

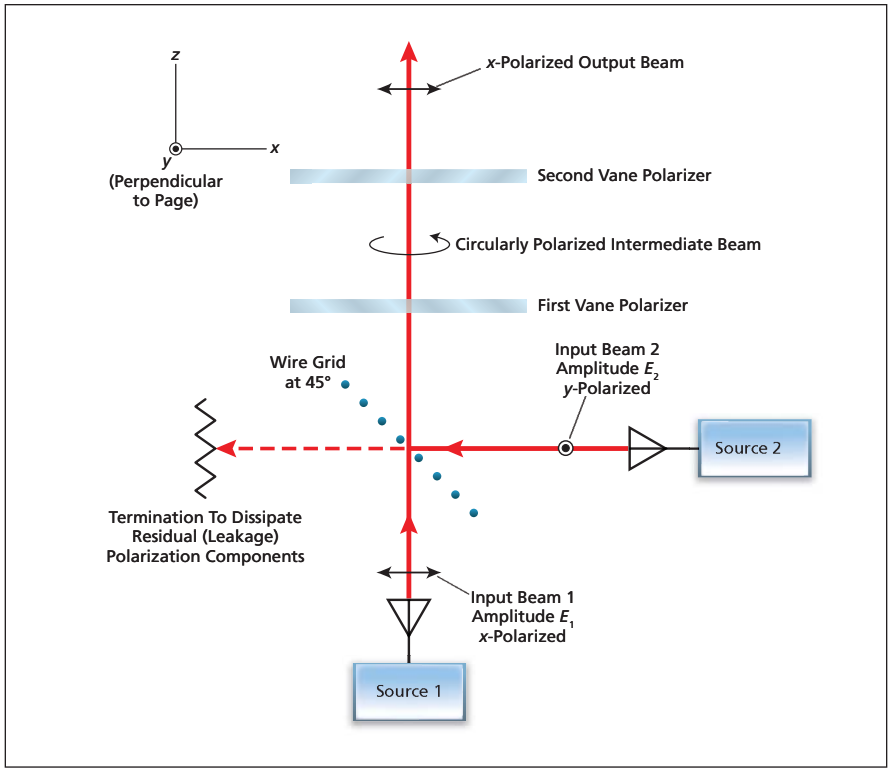

Power From Two Input Beams of possibly unequal amplitude would be combined with minimal loss, provided that the input beams were properly phased and polarized and the vane polarizers were properly positioned and oriented.

path of the wire-grid combiner. The first vane polarizer would be oriented with its vanes at 45° with respect to the polarization of the combined input beam, so that the output of the first vane polarizer would be circularly polarized. The second vane polarizer would convert the circular polarization to linear and would be oriented to place the final output polarization at a desired, standard angle. Fixing the polarization at a standard angle would facilitate the assembly of multiple stages to combine power from more than two sources.

Proper phasing is essential to the success of the proposed scheme. The phasing problem is somewhat more complex than in the case of a simple equal-power combiner because propagation through and between the vane polarizers introduces additional phase shift. However, this is not a serious problem because the majority of the phase shift is a predictable function of the positions and orientations of the vane polarizers, and each power-combining stage could be designed to incorporate an adjustable phase shifter for fine-tuning. There is also an analog of this combining technique in waveguide.

This work was done by Bruce Conroy and Daniel Hoppe of Caltech for NASA's Jet Propulsion Laboratory. Further information is contained in a TSP (see page 1). *NPO-44532*

Synthetic Foveal Imaging Technology

Gigapixel images are analyzed in real time using multiple foveae.

NASA's Jet Propulsion Laboratory, Pasadena, California

Synthetic Foveal imaging Technology (SyFT) is an emerging discipline of image capture and image-data processing that offers the prospect of greatly increased capabilities for real-time processing of large, high-resolution images (including mosaic images) for such purposes as automated recognition and tracking of moving objects of interest. SyFT offers a solution to the image-data-processing problem arising from the proposed development of gigapixel mosaic focal-plane image-detector assemblies for very wide field-of-view imaging with high resolution for detecting and tracking sparse objects or events within narrow subfields of view. In order to identify and track the objects or events without the means of dynamic adaptation to be afforded by SyFT, it would be necessary to post-process data from an image-data space consisting of terabytes of data. Such post-processing would be time-consuming and, as a consequence, could result in missing significant events that could not be observed at all due to the time evolution of such events or could not be observed at required levels of fidelity without such real-time adaptations as adjusting focal-plane operating conditions or aiming of the focal plane in different directions to track such events.

The basic concept of foveal imaging is straightforward: In imitation of a natural eye, a foveal-vision image sensor is designed to offer higher resolution in a small region of interest (ROI) within its field of view. Foveal vision reduces the amount of unwanted information that must be transferred from the image sensor to external image-data-processing circuitry. The aforementioned basic concept is not new in itself: indeed, image sensors based on these concepts have been described in several

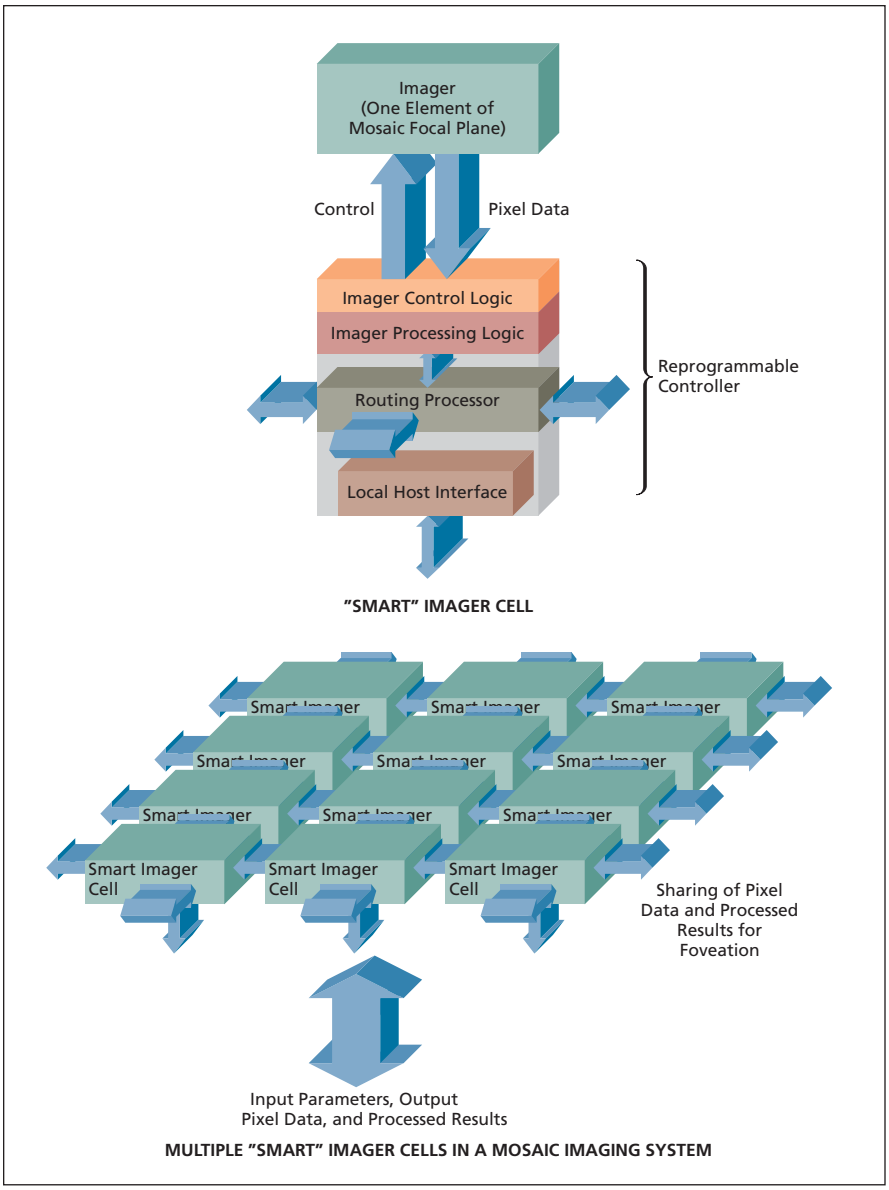

A **Mosaic Imaging System According to SyFT** would be built from "smart" imager cells, each of which would contain a focal-plane image sensor and a reprogrammable controller.

previous *NASA Tech Briefs* articles. Active-pixel integrated-circuit image sensors that can be programmed in real time to effect foveal artificial vision on demand are one such example. What is new in SyFT is a synergistic combination of recent advances in foveal imaging, computing, and related fields, along with a generalization of the basic foveal-vision concept to admit a synthetic fovea that is not restricted to one contiguous region of an image.

The figure depicts a mesh-connected SyFT architecture as applied to a focal-plane mosaic of homogeneous or heterogeneous image sensors. The architecture provides a networked array of reprogrammable controllers for autonomous low-level control with on-the-fly processing of image data from individual image sensors. Each image sensor in the mosaic focal plane is mapped to one of the controllers so that taken together the reprogrammable controllers constitute a conceptual (though not necessarily a geometric) image-processing plane corresponding to the mosaic focal plane. The controllers can be made versatile enough to control and to process pixel data from both charged-coupled-device (CCD) and complementary metal oxide/semiconductor (CMOS) image sensors in the mosaic focal plane. The image sensors can also have multiple pixel data outputs where each output has dedicated processing circuitry in its associated controller to achieve high throughput with real-time processing for feature detection and processing.

Each controller includes a routing processor to implement the network protocol and define the network topology for real-time transfer of raw pixel data and processed results between controllers. The network protocol and the capability to implement it are essential to realization of the capability for synthetic foveal imaging across the entire mosaic focal plane. The processing and networking capabilities of the controllers will enable real-time access to data from multiple image sensors, with application-level control of one or more ROI(s) within the mosaic focal plane array for sharing of detected data features among controllers. These capabilities will effectively facilitate the equivalent of rewiring and reconfiguration with different sensors in the mosaic, with scalability to different mosaic sizes dictated by application requirements. Consequently, the mosaic focal plane is treated as an integrated ensemble of synthetic foveal regions that can traverse the entire mosaic for autonomous intelligent feature detection and tracking capability. Unlike the current state-of-the-art in image sensors, "SyFTing" enables intelligent viewing through vast amounts of image data by treating a mosaic focal plane of sensors as an integrated ensemble rather than a collection of isolated sensors.

This work was done by Michael Hoenk, Steve Monacos, and Shouleh Nikzad of Caltech for NASA's Jet Propulsion Laboratory. Further information is contained in a TSP (see page 1).

In accordance with Public Law 96-517, the contractor has elected to retain title to this invention. Inquiries concerning rights for its commercial use should be addressed to:

Innovative Technology Assets Management
JPL
Mail Stop 202-233
4800 Oak Grove Drive
Pasadena, CA 91109-8099
(818) 354-2240
E-mail: iaoffice@jpl.nasa.gov

Refer to NPO-44209, volume and number of this NASA Tech Briefs *issue, and the page number.*

Airborne Antenna System for Minimum-Cycle-Slip GPS Reception

The antenna is kept pointing upward as the airplane banks.

Goddard Space Flight Center, Greenbelt, Maryland

A system that includes a Global Positioning System (GPS) antenna and associated apparatus for keeping the antenna aimed upward has been developed for use aboard a remote-sensing-survey airplane. The purpose served by the system is to enable minimum-cycle-slip reception of GPS signals used in precise computation of the trajectory of the airplane, without having to restrict the airplane to maneuvers that increase the flight time needed to perform a survey.

"Cycle slip" signifies loss of continuous track of the phase of a signal. Minimum-cycle-slip reception is desirable because maintaining constant track of the phase of the carrier signal from each available GPS satellite is necessary for surveying to centimeter or subcentimeter precision. Even a loss of signal for as short a time as a nanosecond can cause cycle slip. Cycle slips degrade the quality and precision of survey data acquired during a flight.

The two principal causes of cycle slip are weakness of signals and multipath propagation. Heretofore, it has been standard practice to mount a GPS antenna rigidly on top of an airplane, and the radiation pattern of the antenna is typically hemispherical, so that all GPS satellites above the horizon are viewed by the antenna during level flight. When the airplane must be banked for a turn or other maneuver, the reception hemisphere becomes correspondingly tilted; hence, the antenna no longer views satellites that may still be above the Earth horizon but are now below the equatorial plane of the tilted reception hemisphere. Moreover, part of the reception hemisphere (typically, on the inside of a turn) becomes pointed toward ground, with a consequent increase in received noise and, therefore, degradation of GPS measurements.

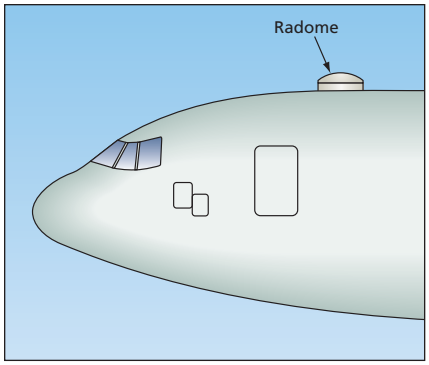

The **Radome Atop the Fuselage** of the NOAA hurricane-hunting airplane houses the present minimum-cycle-slip GPS antenna system.

To minimize the likelihood of loss of signal and cycle slip, bank angles of remote-sensing survey airplanes have generally been limited to 10° or less, resulting in skidding or slipping uncoordinated turns. An airplane must be banked in order to make a coordinated turn. For small-radius, short-time coordinated turns, it is necessary to employ banks as steep as 45°, and turns involving such banks are considered normal maneuvers. These steep banks are highly desirable for minimizing flight

times and for confining airplanes as closely as possible to areas to be surveyed.

The idea underlying the design is that if the antenna can be kept properly aimed, then the incidence of cycle slips caused by loss or weakness of signals can be minimized. The system includes an articulating GPS antenna and associated electronic circuitry mounted under a radome atop an airplane. The electronic circuitry includes a microprocessor-based interface-circuit-and-data-translation module. The system receives data on the current attitude of the airplane from the inertial navigation system of the airplane. The microprocessor decodes the attitude data and uses them to compute commands for the GPS-antenna-articulating mechanism to tilt the antenna, relative to the airplane, in opposition to the roll or bank of the airplane to keep the antenna pointed toward the zenith.

The system was tested aboard the hurricane-hunting airplane of the National Oceanic and Atmospheric Administration (NOAA) [see figure] during an 11-hour flight to observe the landfall of Hurricane Bret in late summer of 1999. No bank-angle restrictions were imposed during the flight. Post-flight analysis of the GPS trajectory data revealed that no cycle slip had occurred.

This work was done by C. Wayne Wright of Goddard Space Flight Center. Further information is contained in a TSP (see page 1).

This invention has been patented by NASA (U.S. Patent No. 6,844,856 B1). Inquiries concerning nonexclusive or exclusive license for its commercial development should be addressed to the Patent Counsel, Goddard Space Flight Center, (301) 286-7351. Refer to GSC-14436-1

Improved Starting Materials for Back-Illuminated Imagers

Thin, highly doped layers are no longer degraded by high-temperature annealing.

NASA's Jet Propulsion Laboratory, Pasadena, California

An improved type of starting materials for the fabrication of silicon-based imaging integrated circuits that include back-illuminated photodetectors has been conceived, and a process for making these starting materials is undergoing development. These materials are intended to enable reductions in dark currents and increases in quantum efficiencies, relative to those of comparable imagers made from prior silicon-on-insulator (SOI) starting materials.

Some background information is prerequisite to a meaningful description of the improved starting materials and process. A prior SOI starting material, depicted in the upper part the figure, includes:

- A device layer on the front side, typically between 2 and 20 μm thick, made of p-doped silicon (that is, silicon lightly doped with an electron acceptor, which is typically boron);
- A buried oxide (BOX) layer (that is, a buried layer of oxidized silicon) between 0.2 and 0.5 μm thick; and
- A silicon handle layer (also known as a handle wafer) on the back side, between about 600 and 650 μm thick.

After fabrication of the imager circuitry in and on the device layer, the handle wafer is etched away, the BOX layer acting as an etch stop. In subsequent operation of the imager, light enters from the back, through the BOX layer. The advantages of back illumination over front illumination have been discussed in prior *NASA Tech Briefs* articles.

For reasons too complex to discuss within the space available for this article, one modification that is necessary for reducing dark current and increasing quantum efficiency is the incorporation of a thin, heavily doped (e.g., p^{++}-doped with boron) silicon layer between the lightly doped device layer and the BOX layer. In prior research, an attempt to incorporate a thin, heavily doped layer by implanting boron at the BOX/device-silicon interface before bonding the BOX layer to the handle wafer did not yield the desired doping profile: The bonding process unavoidably included a high-temperature anneal that caused the implanted boron to diffuse away from the interface, thereby causing an undesired decrease in the doping concentration at the interface and an undesired increase in the doping concentration in the device layer.

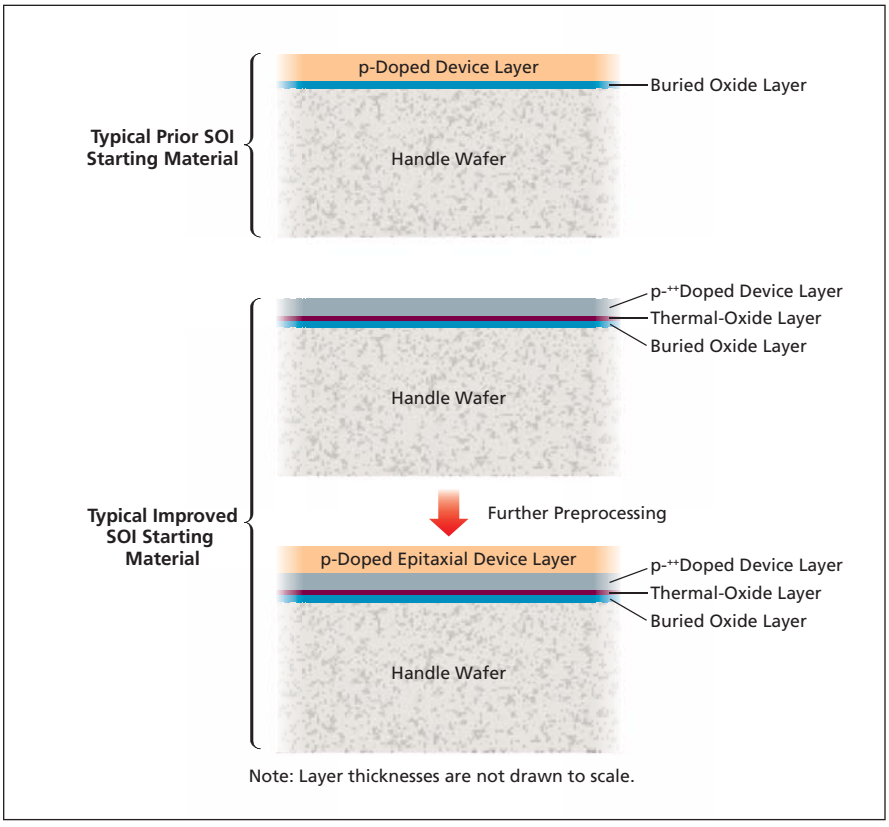

An **SOI Starting Material** of the present improved type differs from a typical prior SOI starting material in several respects.

This concludes the background information.

A starting material of the present improved type, depicted in the middle and lower parts of figure, differs from prior SOI starting materials in the following ways:

- The front silicon layer is heavily doped [e.g., p^{++}-doped with boron], typically at a concentration of 10^{19} atoms/cm^3 instead of being lightly doped at the conventional device concentration of 10^{15} atoms/cm^3.
- There is a layer of thermal oxide between the front silicon layer and the BOX layer.
- The starting material is further preprocessed by growing, to an appropriate thickness, a front epitaxial silicon layer that is lightly doped (e.g., p-doped) typically at a concentration of 7×10^{14} boron atoms/cm^3. This front epitaxial layer serves as the device layer in subsequent fabrication of an imager.

The advantage afforded by such an improved starting material arises from the fact that epitaxial silicon is grown at a temperature much lower than that of the anneal in the aforementioned BOX-to-handle-wafer-bonding process. Therefore, diffusion of boron away from the interface and into the device silicon is prevented. Optionally, one could perform an anneal at an intermediate temperature chosen to effect a small amount of diffusion to optimize the doping profile. Furthermore, the performance of the imager circuitry can be improved because the quality of the epitaxial silicon in the improved starting material is better than that of the float-zone device-layer silicon in prior SOI starting materials. All of the arguments made above would remain valid for cases in which electron-donor (n) dopants were substituted for p dopants.

This work was done by Bedabrata Pain of Caltech for NASA's Jet Propulsion Laboratory. In accordance with Public Law 96-517, the contractor has elected to retain title to this invention. Inquiries concerning rights for its commercial use should be addressed to:

Innovative Technology Assets Management
JPL
Mail Stop 202-233
4800 Oak Grove Drive
Pasadena, CA 91109-8099
(818) 354-2240
E-mail: iaoffice@jpl.nasa.gov

Refer to NPO-41233, volume and number of this NASA Tech Briefs *issue, and the page number.*

Multi-Modulator for Bandwidth-Efficient Communication

Coding and modulation can be selected by loading configuration bits into an FPGA.

NASA's Jet Propulsion Laboratory, Pasadena, California

A modulator circuit board has recently been developed to be used in conjunction with a vector modulator to generate any of a large number of modulations for bandwidth-efficient radio transmission of digital data signals at rates than can exceed 100 Mb/s. The modulations include quadrature phase-shift keying (QPSK), offset quadrature phase-shift keying (OQPSK), Gaussian minimum-shift keying (GMSK), and octonary phase-shift keying (8PSK) with square-root raised-cosine pulse shaping. The figure is a greatly simplified block diagram showing the relationship between the modulator board and the rest of the transmitter. The role of the modulator board is to encode the incoming data stream and to shape the resulting pulses, which are fed as inputs to the vector modulator. The combination of encoding and pulse shaping in a given application is chosen to maximize the bandwidth efficiency.

The modulator board includes gallium arsenide serial-to-parallel converters at its input end. A complementary metal oxide/semiconductor (CMOS) field-programmable gate array (FPGA) performs the coding and modulation computations and utilizes parallel processing in doing so. The results of the parallel computation are combined and converted to pulse waveforms by use of gallium arsenide parallel-to-serial converters integrated with digital-to-analog converters. Without changing the hardware, one can configure the modulator to produce any of the designed combinations of coding and modulation by loading the appropriate bit configuration file into the FPGA.

At the time of reporting the information for this article, a prototype of the modulator board had been tested in lab-

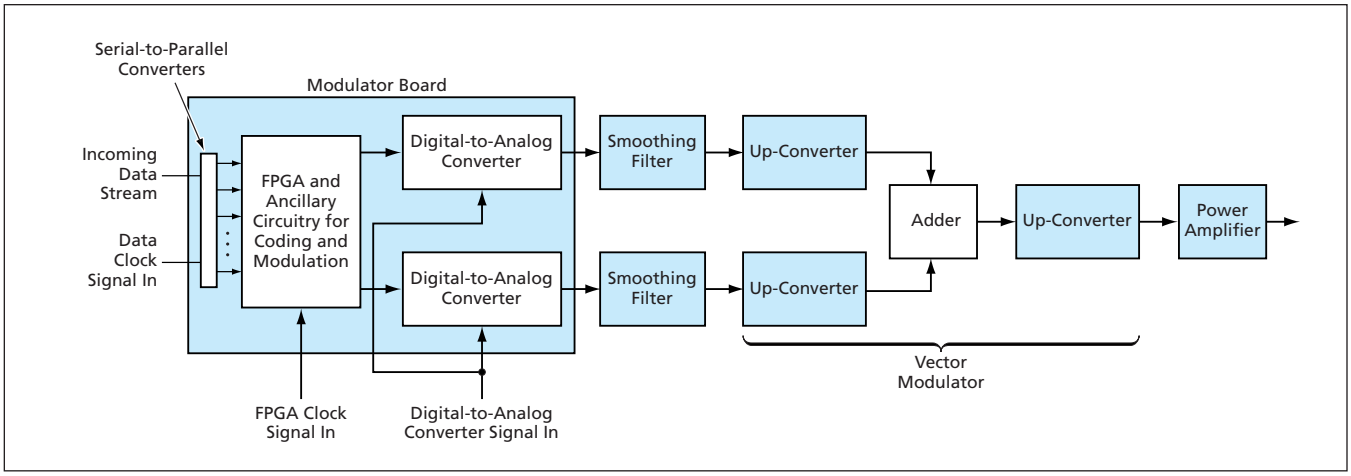

The **Modulator Board** is part of a radio transmitter, wherein it processes an incoming data stream in such a way as to generate modulator inputs for bandwidth-efficient modulation.

oratories, and tests in a two-way ground-to-spacecraft communication link were planned. Although the modulator board was conceived for original use in spacecraft-to-spacecraft and spacecraft-to-ground communications, there are potential terrestrial uses in microwave tower-to-tower links and aircraft remote sensing systems.

By making it possible to implement many different high-rate modulators in the same piece of hardware, the underlying design concepts of this modulator can be expected to afford economies of scale: It would cost less to manufacture many identical modulator hardware units to satisfy market demands for many types of modulators than to manufacture smaller numbers of specialized modulator units having different designs.

This work was done by Andrew Gray, Dennis Lee, Norman Lay, and Craig Cheetham of Caltech; Wai Fong, Pen-Shu Yeh, Robin King, and Parminder Ghuman of Goddard Space Flight Center; and Scott Hoy and Dave Fisher of Lockheed-Martin for NASA's Jet Propulsion Laboratory. Further information is contained in a TSP (see page 1).

In accordance with Public Law 96-517, the contractor has elected to retain title to this invention. Inquiries concerning rights for its commercial use should be addressed to:

Innovative Technology Assets Management
JPL
Mail Stop 202-233
4800 Oak Grove Drive
Pasadena, CA 91109-8099
(818) 354-2240
E-mail: iaoffice@jpl.nasa.gov

Refer to NPO-40807, volume and number of this NASA Tech Briefs *issue, and the page number.*

Some Improvements in Utilization of Flash Memory Devices

Lyndon B. Johnson Space Center, Houston, Texas

Two developments improve the utilization of flash memory devices in the face of the following limitations: (1) a flash write element (page) differs in size from a flash erase element (block), (2) a block must be erased before its is rewritten, (3) lifetime of a flash memory is typically limited to about 1,000,000 erases, (4) as many as 2 percent of the blocks of a given device may fail before the expected end of its life, and (5) to ensure reliability of reading and writing, power must not be interrupted during minimum specified reading and writing times.

The first development comprises interrelated software components that regulate reading, writing, and erasure operations to minimize migration of data and unevenness in wear; perform erasures during idle times; quickly make erased blocks available for writing; detect and report failed blocks; maintain the overall state of a flash memory to satisfy real-time performance requirements; and detect and initialize a new flash memory device.

The second development is a combination of hardware and software that senses the failure of a main power supply and draws power from a capacitive storage circuit designed to hold enough energy to sustain operation until reading or writing is completed.

This work was done by Thomas K. Gender, James Chow, and William E. Ott of Honeywell, Inc., for Johnson Space Center. For further information, contact the Johnson Commercial Technology Office at (281) 483-3809.

Title to this invention has been waived under the provisions of the National Aeronautics and Space Act {42 U.S.C. 2457(f)}, to Honeywell. Inquiries concerning licenses for its commercial development should be addressed to:

Satellite Systems Operation
Honeywell, Inc.
19019 N. 59th Avenue
Glendale, AZ 85308
Phone: (602) 313-5000

Refer to MSC-23465-1/6-1, volume and number of this NASA Tech Briefs *issue, and the page number.*

GPS/MEMS IMU/Microprocessor Board for Navigation

Lyndon B. Johnson Space Center, Houston, Texas

A miniaturized instrumentation package comprising a (1) Global Positioning System (GPS) receiver, (2) an inertial measurement unit (IMU) consisting largely of surface-micromachined sensors of the microelectromechanical systems (MEMS) type, and (3) a microprocessor, all residing on a single circuit board, is part of the navigation system of a compact robotic spacecraft intended to be released from a larger spacecraft [e.g., the International Space Station (ISS)] for exterior visual inspection of the larger spacecraft. Variants of the package may also be useful in terrestrial collision-detection and -avoidance applications.

The navigation solution obtained by integrating the IMU outputs is fed back to a correlator in the GPS receiver to aid in tracking GPS signals. The raw GPS and IMU data are blended in a Kalman filter to obtain an optimal navigation solution, which can be supplemented by range and velocity data obtained by use of (l) a stereoscopic pair of electronic cameras aboard the robotic spacecraft and/or (2) a laser dynamic range imager aboard the ISS. The novelty of the package lies mostly in those aspects of the design of the MEMS IMU that pertain to controlling mechanical resonances and stabilizing scale factors and biases.

This work was done by Ching-Fang Lin of American GNC Corp. for Johnson Space Center. Further information is contained in a TSP (see page 1).

In accordance with Public Law 96-517, the contractor has elected to retain title to this invention. Inquiries concerning rights for its commercial use should be addressed to:

American GNC Corporation
888 Easy Street
Simi Valley CA 93065
Phone No.: (866) 856-8686,
Fax No.: (805) 582-0098
E-mail: marketing@americangnc.com

Refer to MSC-23098-1, volume and number of this NASA Tech Briefs *issue, and the page number.*

T/R Multi-Chip MMIC Modules for 150 GHz

A transmitting gain of 14 dB at 150 GHz has been demonstrated.

NASA's Jet Propulsion Laboratory, Pasadena, California

Modules containing multiple monolithic microwave integrated-circuit (MMIC) chips have been built as prototypes of transmitting/receiving (T/R) modules for millimeter-wavelength radar systems, including phased-array radar systems to be used for diverse purposes that could include guidance and avoidance of hazards for landing spacecraft, imaging systems for detecting hidden weapons, and hazard-avoidance systems for automobiles. Whereas prior landing radar systems have operated at frequencies around 35 GHz, the integrated circuits in this module operate in a frequency band centered at about 150 GHz. The higher frequency (and, hence, shorter wavelength), is expected to make it possible to obtain finer spatial resolution while also using smaller antennas and thereby reducing the sizes and masses of the affected systems.

The integrated circuits contained in the present T/R modules include low-noise amplifiers and power amplifiers previously reported in *NASA Tech Briefs*, variously, as separate chips or modules in "MMIC HEMT Power Amplifier for 140 to 170 GHz" (NPO-30127), Vol. 27, No. 11 (November 2003), page 49; and "Power-Amplifier Module for 145 to 165 GHz" (NPO-40260), Vol. 31, No. 2 (February 2007), page 38. The module housings (see figure) were made from gold-plated brass and include flanges for input and output WR-5 waveguides. [A WR-5 waveguide, nominally designed for operation in the G Band (140 to 220 GHz), has an internal cross section of 0.0510 by 0.0255 in. (about 1.30 by 0.65 mm).]

Each module contains two branches: one for transmitting and one for receiving. Two modules — one containing only the transmitting circuitry, the other containing only the receiving circuitry — were fabricated for initial experiments in which they were tested separately. The transmitting-only module contained two MMIC power-amplifier chips that were fabricated at HRL Laboratories, LLC. The chips were separated by microstrip transmission lines made partly of alumina, and a WR-5 electric-field-plane probe was used to make the transition from the microstrip mode to the waveguide mode. Wire bonds were used to connect the transmission lines to the chips. DC connections were made by means of feedthroughs mounted through the module and connected to bias circuit boards with external multi-pin connectors. At the time of reporting the information for this article, the transmitting-only module had been tested and found to afford about 14 dB of gain over the frequency range from 148 to 150 GHz.

This work was done by Lorene A. Samoska, David M. Pukala, Mary M. Soria, and Gregory A. Sadowy of Caltech for NASA's Jet Propulsion Laboratory. Further information is contained in a TSP (see page 1). ***NPO-46074***

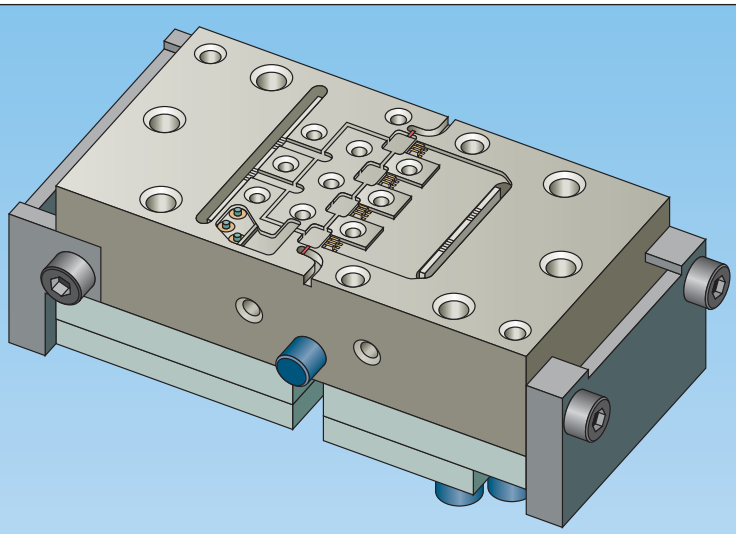

Sketch of Module Housing With Lid Open

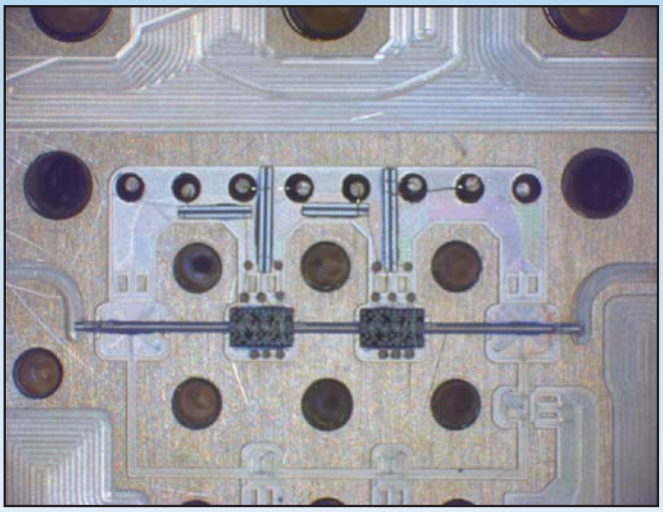

Photograph Showing Input and Output Waveguides, Electric-Field-Plane Transition, Microstrip Lines, and Power-Amplifier MMICs in Transmitting-Only Module

The **Module Housing Contains Cavities** wherein MMIC chips are placed.

Mechanics/Machinery

Pneumatic Haptic Interfaces

Arrays of balloonlike actuators would provide tactile feedback from robot hands.

NASA's Jet Propulsion Laboratory, Pasadena, California

Haptic interfaces in the form of arrays of balloonlike pneumatic actuators are being developed to provide tactile feedback from (1) remote-manipulator hands, tools on the tips of robot arms, and other, similar devices to (2) the hands of human operators. Like other haptic interfaces, these have numerous potential applications in situations in which there are requirements to manipulate remote, very small, and possibly fragile objects with great dexterity and sensitivity. Haptic interfaces are especially valuable as components of robotic implementations of laparoscopic surgical tools, which are used to remotely cut, pull, and move various types of tissue, the degree of softness and hardness of which is difficult or impossible to judge in the absence of tactile feedback.

The figure presents two views of an experimental prototype array that included (1) a molded block of one type of silicone rubber containing holes that define the array of pneumatic actuators and (2) a thin sheet, made of more flexible silicone rubber, bonded to the surface of the block so as to cover the holes. To demonstrate pneumatic actuation, a syringe needle was poked through the block into one of the holes and the syringe plunger was used to force air into the hole, thereby causing the portion of the sheet covering the hole to push outward. In addition, automatic inflation and deflation of the balloon array was demonstrated by using an electronic pressure regulator connected to pressured gas reservoir.

A **Syringe Is Used** to pump air into one of the holes in the block, causing the portion of the sheet covering that hole to protrude to provide a tactile sensation.

After further development, the spatial resolution of the array in a typical application could be expected to be much finer than that shown in the figure — fine enough to enable the device to mimic the shape and texture of an object in contact with a robot hand. In addition, it would be possible to pressurize each hole to the same or a different degree to provide a desired tactile sensation. For example, the pressure in one or more holes could be adjusted to convey a sensation of pressure or force of contact and/or a sense of the hardness of an object in contact with a robot hand. Alternatively or in addition, the pressure in each hole could be varied, independently of the pressures in other holes, as part of a pattern of pressures that could convey a sense of the texture and/or motion of an object.

This work was done by Sam Y. Bae, Victor White, and Harish Manohara of Caltech for NASA's Jet Propulsion Laboratory. Further information is contained in a TSP (see page 1). In accordance with Public Law 96-517, the contractor has elected to retain title to this invention. Inquiries concerning rights for its commercial use should be addressed to:

Innovative Technology Assets Management
JPL
Mail Stop 202-233
4800 Oak Grove Drive
Pasadena, CA 91109-8099
(818) 354-2240
E-mail: iaoffice@jpl.nasa.gov

Refer to NPO-43010, volume and number of this NASA Tech Briefs *issue, and the page number.*

Device Acquires and Retains Rock or Ice Samples

NASA's Jet Propulsion Laboratory, Pasadena, California

The Rock Baller is a sample acquisition tool that improves sample retention. The basic elements of the Rock Baller are the tool rotation axis, the hub, the two jaws, and the cutting blades, which are located on each of the jaws. The entire device rotates about the tool rotation axis, which is aligned parallel to the nominal normal direction of the parent rock surface. Both jaws also rotate about the jaw axis, which is perpendicular to the tool rotation axis, at a rate much slower than the rotation about the tool rotation axis. This movement gradually closes the jaws into a nearly continuous hemispherical shell that encloses the sample as it is cut from the parent rock. When required the jaws are opened to release the sample. The hemispherical cutting method eliminates the sample retention problems associated with existing sample acquisition methods that employ conventional cylindrical cutting.

The resulting samples are hemispher-

ical, or nearly hemispherical, and as a result the aspect ratio (sample depth relative to sample radius) is essentially fixed. This fixed sample aspect ratio may be considered a drawback of the Rock Baller method, as samples with a higher aspect ratio (more depth, less width) may be considered more scientifically valuable because such samples would allow for a broader inspection of the geological record. This aspect ratio issue can be ameliorated if the Rock Baller is paired with a device similar to the Rock Abrasion Tool (RAT) used on the Mars Exploration Rovers. The RAT could be used to first grind into the surface of the parent rock, after which the Rock Baller would extract a sample from a depth inside the rock that would not have been possible without first using the RAT.

Other potential applications for this technology include medical applications such as the removal of tissue samples or tumors from the body, particularly during endoscopic, laparoscopic, or thoracoscopic surgeries.

This work was done by Louis R. Giersch and Paul G. Backes of Caltech for NASA's Jet Propulsion Laboratory. Further information is contained in a TSP (see page 1). ***NPO-46293***

Cryogenic Feedthrough Test Rig

Stennis Space Center, Mississippi

The cryogenic feedthrough test rig (CFTR) allows testing of instrumentation feedthroughs at liquid oxygen and liquid hydrogen temperature and pressure extremes (dangerous process fluid) without actually exposing the feedthrough to a combustible or explosive process fluid. In addition, the helium used (inert gas), with cryogenic heat exchangers, exposes the feedthrough to that environment that allows definitive leak rates of feedthrough by typical industry-standard helium mass spectrometers.

This work was done by Antony Skaff and Daniel Schieb of Sierra Lobo, Inc. for Stennis Space Center.

Inquiries concerning rights for its commercial use should be addressed to:

Antony Skaff
Sierra Lobo, Inc.
11401 Hoover Rd.
Milan, OH 44846
Email: tskaff@sierralobo.com
Telephone: 406-556-9880

Refer to SSC-00299-1, volume and number of this NASA Tech Briefs *issue, and the page number.*

Improved Assembly for Gas Shielding During Welding or Brazing

Inert gas is distributed evenly over the region surrounding the weld joint.

Marshall Space Flight Center, Alabama

An improved assembly for inert-gas shielding of a metallic joint is designed to be useable during any of a variety of both laser-based and traditional welding and brazing processes. The basic purpose of this assembly or of a typical prior related assembly is to channel the flow of a chemically inert gas to a joint to prevent environmental contamination of the joint during the welding or brazing process and, if required, to accelerate cooling upon completion of the process.

In a typical prior welding gas-shielding assembly, depicted in the left part of the figure, the inert gas is fed to the joint through a central nozzle in the welding torch. This arrangement does not always provide adequate protection against contaminants because the inert gas flows turbulently into the joint region and is not evenly distributed in the heated region surrounding the joint. The lack of inert gas in some places in the region surrounding the joint can result in oxidation, which, in turn, can lead to porosity and ultimately to cracking. Improper distribution of shielding gas can also lead to the formation of plasma and to insufficient cooling of portions of the region surrounding the joint that are meant to be protected against excessive heating.

The present improved welding gas-shielding assembly, depicted in the right part of the figure, provides a column of evenly distributed gas flow directly surrounding the pool of molten metal in the weld joint to prevent oxidation and formation of plasma.

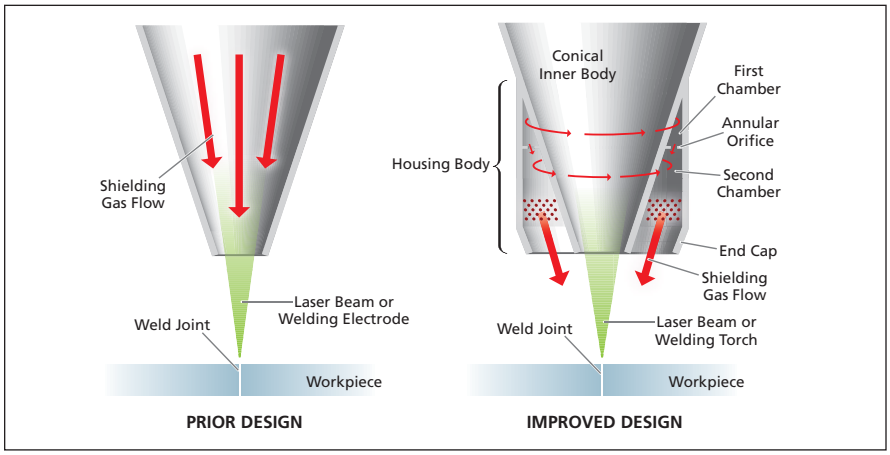

These **Simplified Cross Sections** show the main differences between the present improved welding gas-shielding assembly and a typical prior such assembly.

The assembly includes a conical inner body and an outer shell comprising a housing body and an end cap. The outer shell contains chambers sized and shaped to act, along with the conical inner body, to distribute the inert gas evenly around the conical inner body and to encapsulate the flow of the gas and direct the flow onto the desired region surrounding the weld joint.

The gas enters the assembly through a supply tube from an external source. The passage through which the gas enters is tangential, so the gas flows in tangentially, creating a vortex flow in the chambers between the outer shell and the conical inner body. The gas circulates as it fills the first chamber, then flows through an annular orifice to fill a second chamber and then flows through a series of diffusing screens. After flowing through the screens, the gas is directed to the weld joint area by means of a nozzle. The combination of the vortex flow, chambers, and screens provides even columnar flow around the entire heated area.

This work was done by Paul Gradl and Kevin Baker of Marshall Space Flight Center and Jack Weeks of Pratt & Whitney. For further information, contact Sammy Nabors, MSFC Commercialization Assistance Lead, at sammy.a.nabors@nasa.gov. Refer to MFS-32644-1.

Two-Step Plasma Process for Cleaning Indium Bonding Bumps

This process could increase yields in the manufacture of consumer electronic products.

NASA's Jet Propulsion Laboratory, Pasadena, California

A two-step plasma process has been developed as a means of removing surface oxide layers from indium bumps used in flip-chip hybridization (bump bonding) of integrated circuits. This process has considerable commercial potential in that flip-chip hybridization is used in the manufacture of cellular telephones and other compact, portable electronic products.

The need for this or another, similar cleaning process arises as follows: Indium bonding bumps tend to oxidize during exposure to air. As the duration of exposure and the level of oxidation increase, the electrical resistances of the bonds subsequently formed via the bumps also increase. In some cases, the resistances can become so large that the bump bonds may act as open circuits, preventing proper functioning of the bump-bonded devices.

There is a patented process for removal of surface indium oxide layers by

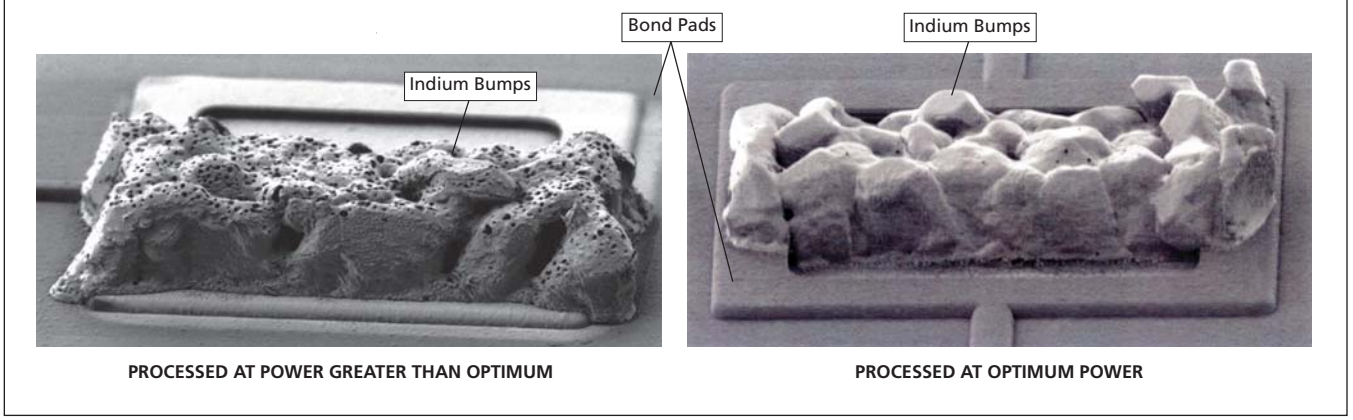

These **Indium Bonding Bumps** were treated by two different versions of the two-step plasma process. The pockmarks on the left bump were caused by using greater-than-optimum plasma-generating power in the second step of the process. The right bump was processed at optimum power.

etching with hydrochloric acid. Unfortunately, once the oxide is removed, the acid can continue to attack the indium, reducing the size of the bumps and even undercutting them. The acid can also attack metal layers on and under the bond pads, potentially creating open circuits and thus negating the benefit of removing the oxide. In contrast, the two-step plasma process makes it possible to remove surface indium oxide, without incurring the adverse effects of the acid etching process.

In the first step of the plasma process, a device on which indium bonding bumps has been formed is exposed for a suitable amount of time (typically, 20 minutes) to a plasma generated in a gaseous mixture of 1/3 argon + 1/3 methane + 1/3 hydrogen. During this step, the oxygen in the indium oxide is removed through incorporation into CO and CO_2 gas molecules, while the indium in the indium oxide is removed through incorporation into $In(CH_3)$, which is volatile. Following this step, a carbonaceous surface film is also formed on device surfaces that are not covered by indium.

A second step for removing the carbonaceous film is as follows. The device is exposed to a plasma generated in a gaseous mixture comprising 72 percent of argon and 28 percent of hydrogen. This step greatly reduces the carbon content without exerting any significant adverse effect on the indium. The power used to generate the plasma in this step must be chosen carefully: the power should be high enough to ensure effective removal of the carbonaceous film, but not so high as to melt or otherwise damage the indium bumps (see figure).

This work was done by Harold F. Greer, Richard P. Vasquez, Todd J. Jones, Michael E. Hoenk, Matthew R. Dickie, and Shouleh Nikzad of Caltech for NASA's Jet Propulsion Laboratory.

In accordance with Public Law 96-517, the contractor has elected to retain title to this invention. Inquiries concerning rights for its commercial use should be addressed to:

Innovative Technology Assets Management
JPL
Mail Stop 202-233
4800 Oak Grove Drive
Pasadena, CA 91109-8099
E-mail: iaoffice@jpl.nasa.gov

Refer to NPO-45911, volume and number of this NASA Tech Briefs *issue, and the page number.*

Tool for Crimping Flexible Circuit Leads

Lyndon B. Johnson Space Center, Houston, Texas

A hand tool has been developed for crimping leads in flexible tails that are parts of some electronic circuits — especially some sensor circuits. The tool is used to cut the tails to desired lengths and attach solder tabs to the leads. For tailoring small numbers of circuits for special applications, this hand tool is a less expensive alternative to a commercially available automated crimping tool. The crimping tool consists of an off-the-shelf hand crimping tool plus a specialized crimping insert designed specifically for the intended application.

The components of the insert and their roles include the following:

- A pin guide aligns pins on the solder tabs with the leads in a tail that is part of the flexible circuit.
- A punch pushes the pins through the pin guide and crimps them onto the tail.
- A forming plate aligns the tail over grooves that form the pins from the solder tabs.
- A spaceplate includes a surface that serves as a stop for positioning the tail when the tail is inserted in the forming plate.
- A dowel pin enables semi-permanent assembly and alignment of the punch, pin guide, and springs.
- A pin holder holds and helps to align the solder tabs before crimping.

This work was done by Aaron Hulse and Myron A. Diftler of Lockheed Martin Corp. for Johnson Space Center. Further information is contained in a TSP (see page 1). ***MSC-23461-1***

$Yb_{14}MnSb_{11}$ as a High-Efficiency Thermoelectric Material

This material could supplant the state-of-the-art material, SiGe.

NASA's Jet Propulsion Laboratory, Pasadena, California

$Yb_{14}MnSb_{11}$ has been found to be well-suited for use as a p-type thermoelectric material in applications that involve hot-side temperatures in the approximate range of 1,200 to 1,300 K. The figure of merit that characterizes the thermal-to-electric power-conversion efficiency is greater for this material than for SiGe, which, until now, has been regarded as the state-of-the art high-temperature p-type thermoelectric material. Moreover, relative to SiGe, $Yb_{14}MnSb_{11}$ is better suited to incorporation into a segmented thermoelectric leg that includes the moderate-temperature p-type thermoelectric material $CeFe_4Sb_{12}$ and possibly other, lower-temperature p-type thermoelectric materials.

Interest in $Yb_{14}MnSb_{11}$ as a candidate high-temperature thermoelectric material was prompted in part by its unique electronic properties and complex crystalline structure, which place it in a class somewhere between (1) a class of semiconducting valence compounds known in the art as Zintl compounds and (2) the class of intermetallic compounds. From the perspective of chemistry, this classification of $Yb_{14}MnSb_{11}$ provides a first indication of a potentially rich library of compounds, the thermoelectric properties of which can be easily optimized.

The concepts of the thermoelectric figure of merit and the thermoelectric compatibility factor are discussed in "Compatibility of Segments of Thermoelectric Generators" (NPO-30798), which appears on page 55. The traditional thermoelectric figure of merit, Z, is defined by the equation

$$Z = \alpha^2/\rho\kappa$$

where α is the Seebeck coefficient, ρ is the electrical resistivity, and κ is the thermal conductivity. Sometimes, in current usage, the term "thermoelectric figure of merit" signifies the product ZT, where T is the absolute temperature. The thermoelectric compatibility factor, s, is defined by the equation

$$s = [(1 + ZT)^{1/2} - 1]/\alpha T.$$

For maximum efficiency, s should not change with temperature, both within a single material, and throughout a segmented thermoelectric-generator leg as a whole. It is in this sense that s serves as a basis for assessing both compatibility among segments and compatibility within a segment (self-compatibility). The degree to which s varies with temperature along a given segment or differs among adjacent segments in a thermoelectric leg thus serves as a measure of incompatibility that one strives to minimize.

As shown in the upper part of the fig-

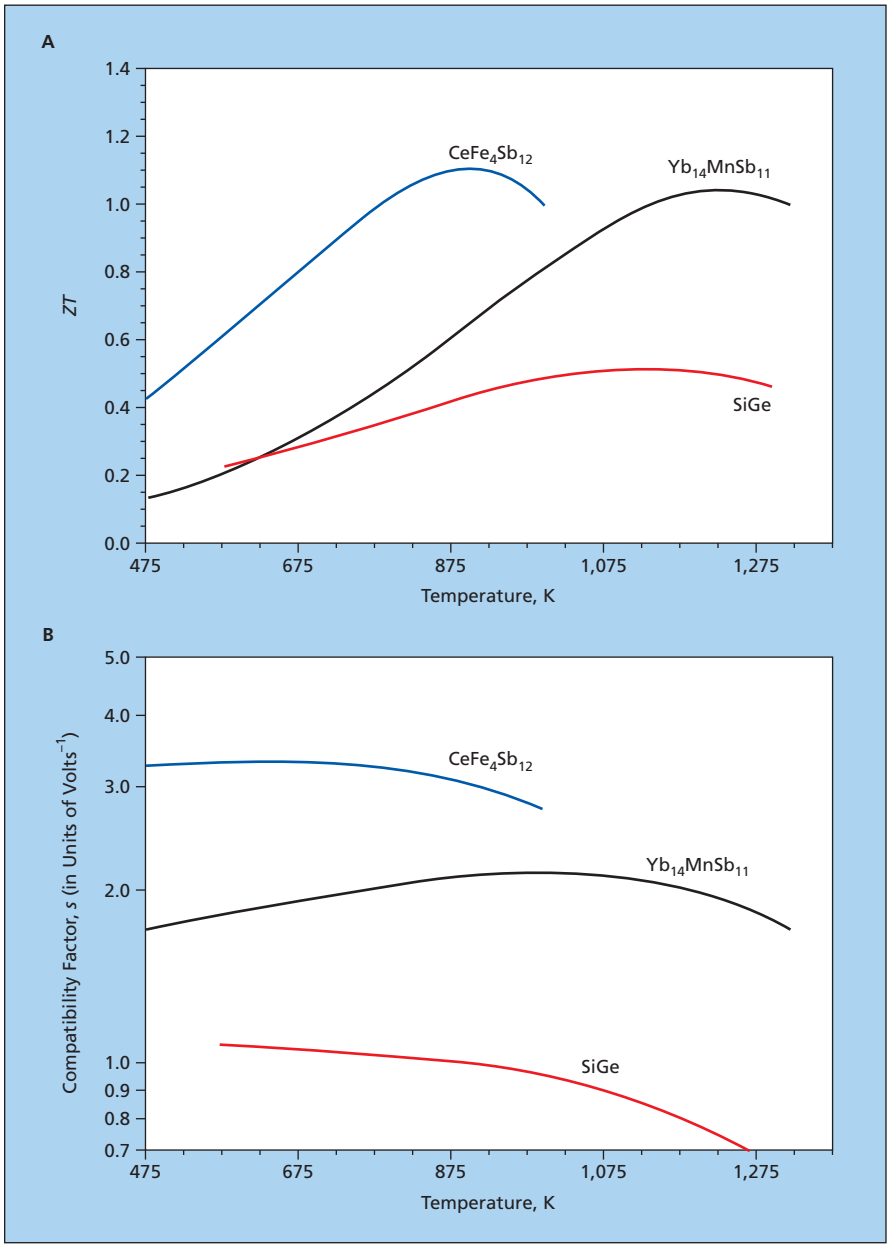

Thermoelectric Figures of Merit and Compatibility Factors of three compounds of interest as functions of temperature are plotted to illustrate the superiority of $Yb_{14}MnSb_{11}$ over SiGe.

ure, in the temperature range of 975 to 1,275 K, the *ZT* value of $Yb_{14}MnSb_{11}$ is approximately double that of SiGe. Moreover, as shown in the lower part of the figure, the *s* value of $Yb_{14}MnSb_{11}$ is much closer to that of $CeFe_4Sb_{12}$ than is the *s* value of SiGe. The net effect of the greater *ZT* and closer match of *s* of $Yb_{14}MnSb_{11}$, compared to those of SiGe, is that the thermal-to-electric power-conversion efficiency of a segmented $Yb_{14}MnSb_{11}/CeFe_4Sb_{12}$ leg operating between the given hot-side and cold-side temperatures is significantly greater than that of a $SiGe/CeFe_4Sb_{12}$ leg operating between the same hot- and cold-side temperatures. For example, for a hot-side temperature of 1,275 K and a cold-side temperature of 775 K, the thermal-to-electric power-conversion efficiency of a segmented $Yb_{14}MnSb_{11}/CeFe_4Sb_{12}$ leg is about 7.3 percent, while that of a segmented $SiGe/CeFe_4Sb_{12}$ leg is about 4.5 percent.

This work was done by G. Jeffrey Snyder and Franck Gascoin of Caltech and Shawna Brown and Susan Kauzlarich of U.C. Davis for NASA's Jet Propulsion Laboratory. In accordance with Public Law 96-517, the contractor has elected to retain title to this invention. Inquiries concerning rights for its commercial use should be addressed to:

Innovative Technology Assets Management
JPL
Mail Stop 202-233
4800 Oak Grove Drive
Pasadena, CA 91109-8099
(818) 354-2240
E-mail: iaoffice@jpl.nasa.gov

Refer to NPO-42627, volume and number of this NASA Tech Briefs *issue, and the page number.*

Polyimide-Foam/Aerogel Composites for Thermal Insulation

These composites may also afford enhanced acoustic attenuation.

John F. Kennedy Space Center, Florida

Composites of specific types of polymer foams and aerogel particles or blankets have been proposed to obtain thermal insulation performance superior to those of the neat polyimide foams. These composites have potential to also provide enhanced properties for vibration dampening or acoustic attenuation. The specific type of polymer foam is denoted "TEEK-H," signifying a series, denoted "H," within a family of polyimide foams that were developed at NASA's Langley Research Center and are collectively denoted "TEEK" (an acronym of the inventors' names).

The specific types of aerogels include Nanogel® aerogel particles from Cabot Corporation in Billerica, MA. and of Spaceloft® aerogel blanket from Aspen Aerogels in Northborough, MA. The composites are inherently flame-retardant and exceptionally thermally stable.

There are numerous potential uses for these composites, at temperatures from cryogenic to high temperatures, in diverse applications that include aerospace vehicles, aircraft, ocean vessels, buildings, and industrial process equipment. Some low-temperature applications, for example, include cryogenic storage and transfer or the transport of foods, medicines, and chemicals. Because of thermal cycling, aging, and weathering most polymer foams do not perform well at cryogenic temperatures and will undergo further cracking over time.

The TEEK polyimides are among the few exceptions to this pattern, and the proposed composites are intended to have all the desirable properties of TEEK-H foams, plus improved thermal performance along with enhanced vibration or acoustic-attenuation performance.

A composite panel as proposed would be fabricated by adding an appropriate amount of TEEK friable balloons into a mold to form a bottom layer. A piece of flexible aerogel blanket material, cut to the desired size and shape, would then be placed on the bottom TEEK layer and sandwiched between another top layer of polyimide friable balloons so that the aerogel blanket would become completely encased in an outer layer of TEEK friable balloons. Optionally, the process could be further repeated to produce multiple aerogel-blanket layers interspersed with and encased by TEEK friable balloons.

The sandwiching of aerogel bulk-fill particles would follow the same methodology or could be mixed directly with friable balloons up to 40% weight loading of the aerogel particles to friable balloons. After sandwiching or mixing of the polymide and aerogel components, the mold, without a top cover, would be placed in a convection furnace and heated at a temperature of 250 °C for one hour. Then the top cover would be placed on the mold and the temperature increased to about 320 °C for between 1 and 3 hours for full imidization of the polyimide component. The resulting composite should have all the desirable properties of TEEK, and its effective thermal conductivity should be less than that of an approximately equally dense panel made of TEEK foam only. The heat transfer reduction is directly proportional to % loading of the aerogel component. The excellent structural integrity of the foam material is maintained in the composite formulations.

This work was done by Martha Williams, James Fesmire, Jared Sass and Trent Smith of Kennedy Space Center and Erik Weiser of Langley Research Center. For further information, contact the Kennedy Innovative Partnerships Office at (321) 861-7158. KSC-12894

Converting CSV Files to RKSML Files

A computer program converts, into a format suitable for processing on Earth, files of downlinked telemetric data pertaining to the operation of the Instrument Deployment Device (IDD), which is a robot arm on either of the Mars Explorer Rovers (MERs). The raw downlinked data files are in comma-separated-value (CSV) format. The present program converts the files into Rover Kinematics State Markup Language (RKSML), which is an Extensible Markup Language (XML) format that facilitates representation of operations of the IDD and enables analysis of the operations by means of the Rover Sequencing Validation Program (RSVP), which is used to build sequences of commanded operations for the MERs.

After conversion by means of the present program, the downlinked data can be processed by RSVP, enabling the MER downlink operations team to play back the actual IDD activity represented by the telemetric data against the planned IDD activity. Thus, the present program enhances the diagnosis of anomalies that manifest themselves as differences between actual and planned IDD activities.

This program was written by Ashitey Trebi-Ollennu and Robert Liebersbach of Caltech for NASA's Jet Propulsion Laboratory.

This software is available for commercial licensing. Please contact Karina Edmonds of the California Institute of Technology at (626) 395-2322. Refer to NPO-44682.

Service Management Database for DSN Equipment

This data- and event-driven persistent storage system leverages the use of commercial software provided by Oracle for portability, ease of maintenance, scalability, and ease of integration with embedded, client-server, and multi-tiered applications. In this role, the Service Management Database (SMDB) is a key component of the overall end-to-end process involved in the scheduling, preparation, and configuration of the Deep Space Network (DSN) equipment needed to perform the various telecommunication services the DSN provides to its customers worldwide.

SMDB makes efficient use of triggers, stored procedures, queuing functions, e-mail capabilities, data management, and Java integration features provided by the Oracle relational database management system. SMDB uses a third normal form schema design that allows for simple data maintenance procedures and thin layers of integration with client applications. The software provides an integrated event logging system with ability to publish events to a JMS messaging system for synchronous and asynchronous delivery to subscribed applications. It provides a structured classification of events and application-level messages stored in database tables that are accessible by monitoring applications for real-time monitoring or for troubleshooting and analysis over historical archives.

SMDB maintains a relatively small footprint of online data to maximize performance and minimize MTTR (mean time to repair) in case of failure. It also integrates Java, PL/SQL, and C codes to implement workflow rules, data processing, and data transformation functions invoked by data change events and timer events. Generic timer functions are implemented that are capable of delivering any type of message to a registered timer event processing function. SMDB exposes a set of APIs (application programming interfaces) for the retrieval, insert, and update of various types of structured data.

SMDB replaces an old file-based system driven by labor-intensive processes. It prompts for missing input and warns users and operators when this occurs. SMDB automatically generates the products needed to configure ground equipment and takes care of distributing the products to the DSN local and remote sites. It maintains a manageable size by automatically moving older data to an archiving subsystem and allows for controlled online software updates to reflect new processing rules or additional processing functions.

This work was done by Silvino Zendejas, Tung Bui, Bach Bui, Shantanu Malhotra, Fannie Chen, Paul Wolgast, Christopher Allen, Ivy Luong, George Chang, and Syed Sadaqathulla of Caltech for NASA's Jet Propulsion Laboratory.

This software is available for commercial licensing. Please contact Karina Edmonds of the California Institute of Technology at (626) 395-2322. Refer to NPO-45013.

Chemochromic Hydrogen Leak Detectors

Robust, simple, and easy-to-detect, color-changing hydrogen sensors warn against explosion hazard.

John F. Kennedy Space Center, Florida

At NASA, hydrogen safety is a key concern for space shuttle processing. Leaks of any level must be quickly recognized and addressed due to hydrogen's lower explosion limit. Chemochromic devices have been developed to detect hydrogen gas in several embodiments. Because hydrogen is odorless and colorless and poses an explosion hazard, there is an emerging need for sensors to quickly and accurately detect low levels of leaking hydrogen in fuel cells and other advanced energy-generating systems in which hydrogen is used as fuel.

The device incorporates a chemochromic pigment into a base polymer. The article can reversibly or irreversibly change color upon exposure to hydrogen. The irreversible pigment changes color from a light beige to a dark gray. The sensitivity of the pigment can be tailored to its application by altering its exposure to gas through the incorporation of one or more additives or polymer matrix. Furthermore, through the incorporation of insulating additives, the chemochromic sensor can operate at cryogenic temperatures as low as 78 K.

A chemochromic detector of this type can be manufactured into any feasible polymer part including injection molded plastic parts, fiber-spun textiles, or extruded tapes. The detectors are simple, inexpensive, portable, and do not require an external power source. The chemochromic detectors were installed and removed easily at the KSC launch pad without need for special expertise. These detectors may require an external monitor such as the human eye, camera, or electronic detector; however, they could be left in place, unmonitored, and examined later for color change to determine whether there had been exposure to hydrogen.

In one type of envisioned application, chemochromic detectors would be fabricated as outer layers (e.g., casings or coatings) on high-pressure hydrogen storage tanks and other components of hydrogen-handling systems to provide visible indications of hydrogen leaks caused by fatigue failures or other failures in those systems. In another type of envisioned application, chemochromic detectors of this type could be optoelectronically instrumented for monitoring to provide measured digital indications of color changes indicative of the presence of hydrogen.

This work was done by Luke Roberson, Janine Captain, Martha Williams, Trent Smith, and LaNetra Tate of Kennedy Space Center; and Ali Raissi, Nahid Mohajeri, Nazim Muradov, and Gary Bokerman of Florida Solar Energy Center. For additional information, contact the Kennedy Space Center Innovative Partnerships Program Office at (321) 861-7158. KSC-13088

Compatibility of Segments of Thermoelectric Generators

A compatibility factor that depends only on material and temperature has been defined.

NASA's Jet Propulsion Laboratory, Pasadena, California

A method of calculating (usually for the purpose of maximizing) the power-conversion efficiency of a segmented thermoelectric generator is based on equations derived from the fundamental equations of thermoelectricity. Because it is directly traceable to first principles, the method provides physical explanations in addition to predictions of phenomena involved in segmentation. In comparison with the finite-element method used heretofore to predict (without being able to explain) the behavior of a segmented thermoelectric generator, this method is much simpler to implement in practice: in particular, the efficiency of a segmented thermoelectric generator can be estimated by evaluating equations using only handheld calculator with this method. In addition, the method provides for determination of cascading ratios. The concept of cascading is illustrated in the figure and the definition of the "cascading ratio" is defined in the figure caption.

An important aspect of the method is its approach to the issue of compatibility among segments, in combination with introduction of the concept of compatibility within a segment. Prior approaches involved the use of only averaged material properties. Two materials in direct contact could be examined for compatibility with each other, but there was no general framework for analysis of compatibility. The present method establishes such a framework.

The mathematical derivation of the method begins with the definition of reduced efficiency of a thermoelectric generator as the ratio between (1) its thermal-to-electric power-conversion efficiency and (2) its Carnot efficiency (the maximum efficiency theoretically attainable, given its hot- and cold-side temperatures). The derivation involves calculation of the reduced efficiency of a model thermoelectric generator for which the hot-side temperature is only infinitesimally greater than the cold-side temperature. The derivation includes consideration of the ratio (u) between the electric current and heat-conduction power and leads to the concept of compatibility factor (s) for a given thermoelectric material, defined as the value of u that maximizes the reduced efficiency of the aforementioned model thermoelectric generator. It turns out that s depends only on the absolute temperature (T) and on intrinsic properties of the ma-

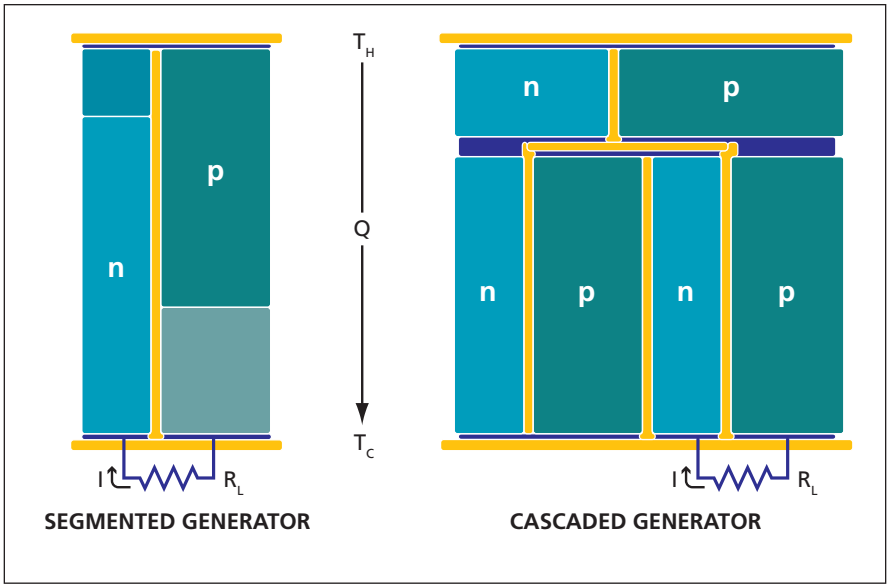

This **Schematic Diagram** compares segmented with cascaded thermoelectric generator. The cascading ratio is defined as the ratio between the numbers of unicouples in the two stages.

terial that may vary with the temperature. The equation for s is

$$s \equiv \frac{\sqrt{1+ZT}-1}{\alpha T}$$

where Z is the traditional thermoelectric figure of merit, defined as $Z = \alpha^2/\rho\kappa$; α is the Seebeck coefficient; ρ is the electrical resistivity; and κ is the thermal conductivity.

For maximum efficiency, u should be equal to s, both within a single material, and throughout a segmented thermoelectric-generator leg as a whole. It is in this sense that s serves as a basis for assessing both compatibility among segments and compatibility within a segment (self-compatibility). Given that u remains relatively constant throughout the thermoelectric element, the degree to which s varies with temperature along a given segment or differs among adjacent segments thus serves as a measure of incompatibility that one strives to minimize.

The compatibility factor can further be used as a quantitative guide for deciding whether a thermoelectric material is better suited for segmentation or cascading. Cascading enables the use of a material that may be suitable for a given temperature stage but is incompatible for segmentation with one or more other materials in the same temperature stage. The simplest option that may be available in a given case is to choose the numbers of unicouples in both temperature stages such that each stage is operating at its optimal u value. Such a choice is embodied in the following expression for the cascading ratio:

$$\frac{g'}{g} = \frac{u'}{u}$$

where g is the number of unicouples per stage and the prime mark distinguishes one stage from the other.

This work was done by G. Jeffrey Snyder and Tristan Ursell of Caltech for NASA's Jet Propulsion Laboratory. For more information, contact iaoffice@jpl.nasa.gov. NPO-30798

Complementary Barrier Infrared Detector

These detectors can be used in infrared imaging cameras in manufacturing process monitoring, environmental monitoring, and medical imaging.

NASA's Jet Propulsion Laboratory, Pasadena, California

The complementary barrier infrared detector (CBIRD) is designed to eliminate the major dark current sources in the superlattice infrared detector. The concept can also be applied to bulk semiconductor-based infrared detectors. CBIRD uses two different types of specially designed barriers: an electron barrier that blocks electrons but not holes, and a hole barrier that blocks holes but not electrons. The CBIRD structure consists of an n-contact, a hole barrier, an absorber, an electron barrier, and a p-contact.

The barriers are placed at the contact-absorber junctions where, in a conventional p-i-n detector structure, there normally are depletion regions that produce generation-recombination (G-R) dark currents due to Shockley-Read-Hall (SRH) processes. The wider-

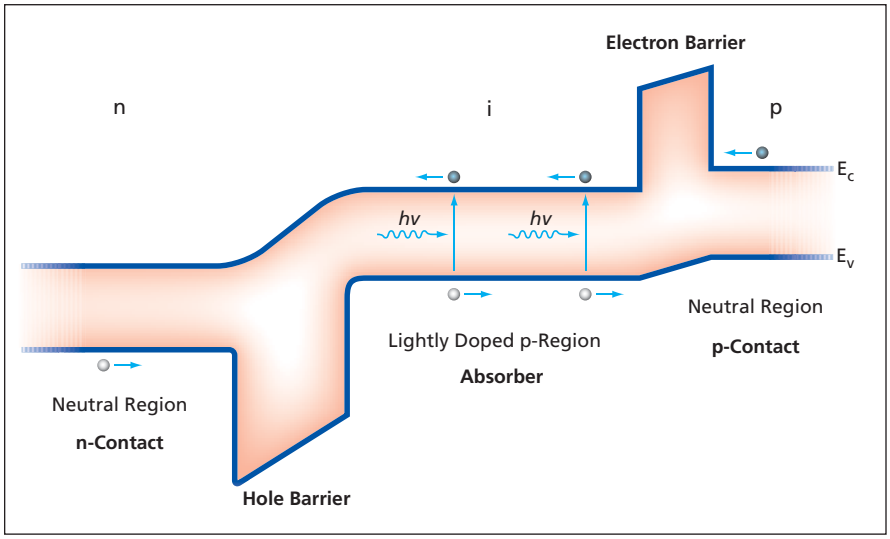

This schematic energy band diagram illustrates the **Complementary Barrier Infrared Detector** (CBIRD) concept.

bandgap complementary barriers suppress G-R dark current. The barriers also block diffusion dark currents generated in the diffusion wings in the neutral regions. In addition, the wider gap barriers serve to reduce tunneling dark currents. In the case of a superlattice-based absorber, the superlattice itself can be designed to suppress dark currents due to Auger processes. At the same time, the barriers actually help to enhance the collection of photo-generated carriers by deflecting the photo-carriers that are diffusing in the "wrong" direction (i.e., away from collectors) and redirecting them toward the collecting contacts. The contact layers are made from materials with narrower bandgaps than the barriers. This allows good ohmic contacts to be made, resulting in lower contact resistances.

Previously, THALES Research and Technology (France) demonstrated detectors with bulk InAsSb (specifically $InAs_{0.91}Sb_{0.09}$) absorber lattice-matched to GaSb substrates. The absorber is surrounded by two wider bandgap layers designed to minimize impedance to photocurrent flow. The wide bandgap materials also serve as contacts. The cutoff wavelength of the InAsSb absorber is fixed. CBIRD may be considered as a modified version of the THALES double heterostructure (DH) p-i-n device, but with even wider bandgap barriers inserted at the contact layer/absorber layer interfaces. It is designed to work with either bulk semiconductors or superlattices as the absorber material. The superlattice bandgap can be adjusted to match the desired absorption cutoff wavelength.

This infrared detector has the potential of high-sensitivity operation at higher operating temperatures. This would reduce cooling requirements, thereby reducing the power, mass, and volume of the equipment and allowing an increased mission science return.

This work was done by David Z. Ting, Sumith V. Bandara, Cory J. Hill, and Sarath D. Gunapala of Caltech for NASA's Jet Propulsion Laboratory. Further information is contained in a TSP (see page 1).

In accordance with Public Law 96-517, the contractor has elected to retain title to this invention. Inquiries concerning rights for its commercial use should be addressed to:

Innovative Technology Assets Management
JPL
Mail Stop 202-233
4800 Oak Grove Drive
Pasadena, CA 91109-8099
E-mail: iaoffice@jpl.nasa.gov

Refer to NPO-46207, volume and number of this NASA Tech Briefs *issue, and the page number.*

JPL Greenland Moulin Exploration Probe

NASA's Jet Propulsion Laboratory, Pasadena, California

A probe was designed to investigate the moulins (melt water drainage channels on an ice cap) and ice-hydrology interaction in the Greenland Ice Cap. By using commercially available components, the strong and reliable system has been developed that has a high-definition video recording element, is lightweight, and has buoyancy that is easily adjustable for neutrality or to be slightly positive in the water, enabling different deployment scenarios.

The system is in a small (20×20×20-cm), watertight Lexan box that can follow the water into the ice, but then be retrieved by tether. The system is rated for a water depth of 100 meters. The purpose of this system is to gain understanding about the interaction between the ice and the melt water and how this interaction may be accelerating the melting of glaciers and, in general, an overall better understanding of global warming.

This work was done by Alberto Behar and Victor Zlotnicki of Caltech; Huan Wang of Stanford; Henrik Karlsson of the International Space University; Jonas Jonsson of Angstrom Space Laboratory; and Konrad Steffen and Russell Huff of the University of Colorado, Boulder, for NASA's Jet Propulsion Laboratory. For more information, contact iaoffice@jpl.nasa.gov. NPO-45464

Books & Reports

Ultra-Lightweight Self-Deployable Nanocomposite Structure for Habitat Applications

A document discusses self-deployable, rigidized structures that are ultra-lightweight and have gas barrier properties, space durability, and high impact resistance. Developed here are microcellular-foamed sandwich structures made from nanocomposite shape memory polymers (SMPs) with Cold-Hibernated Elastic Memory (CHEM) deployed technique for space structural components including space habitats. This type of foam sandwich also does not suffer from the toxicity problems of conventional foams, and has higher mechanical properties than those processed with conventional techniques. This design can be compacted into a very small volume for launch. Once deployed, the microcellular structure can use the heat from the Sun to recover 98 to 100 percent of its shape.

This work was done by Seng C. Tan of Wright Materials Research Corp. for Johnson Space Center. Further information is contained in a TSP (see page 1).

In accordance with Public Law 96-517, the contractor has elected to retain title to this invention. Inquiries concerning rights for its commercial use should be addressed to:

Wright Materials Research Co.
1187 Richfield Center
Beavercreek, OH 45430
Phone No.: (937) 431-8811
Fax: (937) 431-4746

Refer to MSC-24290-1, volume and number of this NASA Tech Briefs *issue, and the page number.*

Room-Temperature Ionic Liquids for Electrochemical Capacitors

A document discusses room-temperature ionic liquids (RTILs) used as electrolytes in carbon-nanotube-based, electrochemical, double-layer capacitors. Unlike the previous electrolyte (EtNB4 in acetonitrile), the RTIL used here does not produce cyanide upon thermal decomposition and does not have a moisture sensitivity.

This work was done by Heather Fireman, Leonard Yowell, and Padraig G. Moloney of Johnson Space Center; Sivaram Arepalli, P. Nikolaev, and C. Huffman of ERC, Inc.; Jud Ready, C.D. Higgins, S. P. Turano, P. A. Kohl, and K. Kim of Georgia Tech Research Institute. Further information is contained in a TSP (see page 1). MSC-24190-1

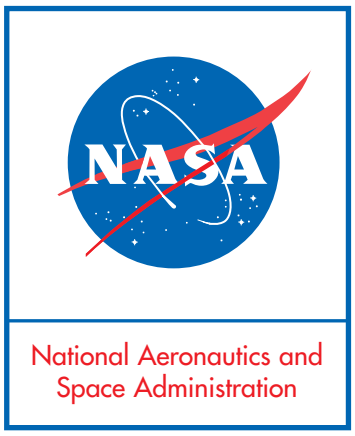
NASA
National Aeronautics and
Space Administration